

Department of Chemistry and Materials Science

Luminescent markers and labels in authentication and novel bioaffinity assays

Päivi Grönroos

Luminescent markers and labels in authentication and novel bioaffinity assays

Päivi Grönroos

The public defense on 8th May 2020 at 12:00 will be organized via remote technology.

Link: <https://aalto.zoom.us/j/67255691803>

Zoom Quick Guide: <https://www.aalto.fi/en/services/zoom-quick-guide>

A doctoral dissertation completed for the degree of Doctor of Science (Technology) to be defended, with the permission of the Aalto University School of Chemical Engineering, at a public examination held at the lecture hall Ke2 of the school on 8 May 2020 at 12.

**Aalto University
School of Chemical Engineering
Department of Chemistry and Materials Science
Analytical Chemistry**

Supervising professor

Prof. Sakari Kulmala, Aalto University, Finland

Thesis advisor

Prof. Sakari Kulmala, Aalto University, Finland

Preliminary examiners

Prof. Tero Soukka, University of Turku, Finland

Prof. Igor Koshevoy, University of Eastern Finland, Finland

Opponent

Prof. Pekka Hänninen, University of Turku, Finland

Aalto University publication series

DOCTORAL DISSERTATIONS 53/2020

© 2020 Päivi Grönroos

ISBN 978-952-60-3820-9 (printed)

ISBN 978-952-60-3821-6 (pdf)

ISSN 1799-4934 (printed)

ISSN 1799-4942 (pdf)

<http://urn.fi/URN:ISBN:978-952-60-3821-6>

Painosalama Oy

Turku 2020

Finland



Printed matter
4041-0619

Author

Päivi Grönroos

Name of the doctoral dissertation

Luminescent markers and labels in authentication and novel bioaffinity assays

Publisher School of Chemical Engineering**Unit** Department of Chemistry and Materials Science**Series** Aalto University publication series DOCTORAL DISSERTATIONS 53/2020**Field of research** Analytical Chemistry**Manuscript submitted** 12 February 2020**Date of the defence** 8 May 2020**Permission for public defence granted (date)** 18 March 2020**Language** English **Monograph** **Article dissertation** **Essay dissertation****Abstract**

Luminescence can be utilized in various commercially important applications such as anti-counterfeit (AC) markings and bioaffinity assays. The increasing demands for product authentication by consumers, and point-of-care (POC) health monitoring systems, can be met using luminescence based solutions developed to be compatible with simple instrumentation such as smartphones. Use of environmentally friendly materials like cellulose would further benefit such applications.

In this thesis, the luminescence properties of fibrillary cellulose films and cardboard materials are studied to find a cellulose based material usable as a substrate for luminescent AC markers. Multiple combinations of organic luminophores, lanthanide chelates and inorganic phosphors have been used to create datasets i.e. luminescence topography maps (LTM) for verification of the authenticity of the product package. The whole authentication process, from the photoexcitation of the marker to the recognition of the product, is demonstrated with a smartphone application. Wide variety of marker luminophores can be used in the future, as camera technologies and computing power of the smartphones are constantly evolving. The results also show that cellulose as substrate displays weak long-lived photoluminescence emission. This emission originating from multiple luminescence centers, can be utilized in LTM as an internal standard in the method.

Cellulose based composite materials are also investigated as low-cost alternatives for expensive oxide-coated silicon electrodes for electrochemiluminoimmunoassays. Composite electrodes made of insulating cellulose derivatives or polystyrene with different conductive carbon materials are studied, and these materials are used to make screen-printed electrode chips. The analytical applicability of the electrodes have been tested in immunoassay of C-reactive protein with Tb(III)chelate and fluorescein isothiocyanate (FITC) labels. The results indicate that conductive carbon-cellulose composite materials are well suited for the fabrication of screen-printed electrodes. Low background emission, wide linear range and low detection limits are obtained with these electrodes. FITC could provide lower detection limits of the analyte than the presently used Tb(III) chelate labels, which is very promising for low-cost POCT applications.

Keywords Luminophores, Authentication, Cellulose, Composite electrodes, Bioaffinity assays**ISBN (printed)** 978-952-60-3820-9**ISBN (pdf)** 978-952-60-3821-6**ISSN (printed)** 1799-4934**ISSN (pdf)** 1799-4942**Location of publisher** Helsinki**Location of printing** Turku**Year** 2020**Pages** 125**urn** <http://urn.fi/URN:ISBN:978-952-60-3821-6>

Tekijä

Päivi Grönroos

Väitöskirjan nimi

Luminoivat merkki- ja leima-aineet autentikoinnissa ja bioaffiniteettimäärityksissä

Julkaisija Kemian tekniikan korkeakoulu**Yksikkö** Kemian ja materiaalitieteen laitos**Sarja** Aalto University publication series DOCTORAL DISSERTATIONS 53/2020**Tutkimusala** Analyytinen kemia**Käsikirjoituksen pvm** 12.02.2020**Väitöspäivä** 08.05.2020**Väittelyluvan myöntämispäivä** 18.03.2020**Kieli** Englanti **Monografia** **Artikkeliväitöskirja** **Esseeväitöskirja****Tiivistelmä**

Luminesenssia voidaan hyödyntää useissa kaupallisesti merkittävässä sovelluksissa, kuten väärennösten ehkäisyssä ja bioaffiniteettimäärityksissä. Pienlaitteilla tehtävä vierianalytiikka ja tuotteiden aitouden varmentavat menetelmät ovat tulleet kaiken aikaa yhä merkittävimmiksi, ja kuluttajien itse käyttämät pienlaitteet tulevat olemaan tulevaisuudessa hyvin tärkeässä asemassa. Luminesenssiin perustuva määritysmenetelmä, joka on kehitetty yhteensopivaksi yksinkertaisten laitteistojen, kuten älypuhelinien kanssa, vastaa varsin pitkälti näihin vaatimuksiin. Ympäristöystävällisten valmistusmateriaalien, kuten selluloosan käyttö edistää myös osaltaan sovellusten kiinnostavuutta.

Väitöskirjatyössä tutkittiin fibrilliseluloosakalvojen ja kartonkimateriaalien luminesenssiominaisuuksia sekä niiden hyödynnettävyyttä substraateina luminoiville merkkiaineille. Useiden orgaanisten luminoforien, lantanidikelaattien ja epäorgaanisten fosforien yhdistelmiä hyödynnettiin aitouden varmentamiseen käytettävissä tietokannoissa luminesenssitopografiakarttojen muodossa. Koko aitouden tarkistamisprosessi, merkinnän valovirityksestä tuotteen tunnistamiseen, toteutettiin myös älypuhelinsovelluksella. Laajaa valikoimaa erilaisia merkkiaineita voidaan hyödyntää tulevaisuudessa älypuhelinien kameratekniikan ja laskentatehon kehittyessä. Selluloosalla havaittiin esiintyvän useasta luminesenssikeskuksesta johtuvaa pitkäikäistä luminesenssia, jota voidaan myös tarvittaessa hyödyntää aitousmerkinnän pakkausmateriaalikohtaisena sisäisenä standardina.

Väitöskirjatyössä tutkittiin myös selluloosapohjaisista komposiittimateriaaleista valmistettuja elektrodeja edullisina vaihtoehtoina oksidipäällystetyille piielektrodeille elektrokemiluminoimismäärityksissä. Selluloosajohdannaisia ja polystyreeniä käytettiin eristemateriaalina, ja hiilimustaa ja grafiittia johdemateriaalina komposiittimusteissa, joista valmistettiin silkkipainettuja elektrodisiruja. Elektrodien analyytinen sovellettavuus testattiin C-reaktiivisen proteiinin määrittämisellä käytettäessä leima-aineina Tb(III)kelaattia ja fluoreseiini-isotiosyanaattia (FITC). Selluloosapohjaiset komposiittimateriaalit soveltuvat hyvin silkkipainettujen elektrodien valmistukseen, ja niillä todettiin olevan matala taustaemissio, laaja lineaarinen alue ja matalat toteamisrajat. FITC:llä voidaan saada jopa matalampia toteamisrajoja kuin Tb(III)kelaatilla, mikä on lupaava ominaisuus kustannuksiltaan edullisia vierianalytiikan sovelluksia ajatellen.

Avainsanat Luminoforit, Autentikointi, Selluloosa, Komposiittielektrodit, Bioaffiniteettimääritykset**ISBN (painettu)** 978-952-60-3820-9**ISBN (pdf)** 978-952-60-3821-6**ISSN (painettu)** 1799-4934**ISSN (pdf)** 1799-4942**Julkaisupaikka** Helsinki**Painopaikka** Turku**Vuosi** 2020**Sivumäärä** 125**urn** <http://urn.fi/URN:ISBN:978-952-60-3821-6>

Acknowledgements

The research work presented within this thesis was carried out in the Research group of Analytical Chemistry, Department of Chemistry and Materials Science, Aalto University. Tekes, Aalto University, Biometro, Labmaster, and Jenny and Antti Wihuri Foundation are gratefully acknowledged for the financial support of my work.

I want to thank my supervising professor Sakari Kulmala and my colleague Dr. Kalle Salminen from the research group of Analytical Chemistry, and prof. Jouni Paltakari and Mr. Marko Raatikka who were in the same project team with me during the LuminoTrace project. I also want to thank all those interesting people I have been privileged to know and work with during my years at Aalto University.

Special thanks to my family and friends. I hope you all know how important you are to me.

Ellille

Helsinki, March 2020

Päivi Grönroos

Contents

List of Abbreviations and Symbols	iii
List of Publications	v
Author's Contribution.....	vi
1. Introduction	1
2. Principles of Luminescence.....	3
2.1 Photoluminescence.....	3
2.2 Hot electron-induced electrochemiluminescence	4
3. Luminescent labels and markers.....	6
3.1 Organic luminophores and metal chelates.....	7
3.2 Persistent luminescence phosphors	8
3.3 Luminescent markers in anti-counterfeit applications	10
4. Cellulose as a material in luminescence applications	12
4.1 Basics of cellulose	12
4.2 Applications of cellulose.....	13
5. Electrode materials for hot electron electrochemistry	15
5.1 Metal electrodes	15
5.2 Thin insulating film-coated electrodes.....	16
5.3 Applications of HECL in bioaffinity assays	17
6. Experimental.....	19
6.1 Photoluminescence studies	19
6.1.1 Fibrillar cellulose films and cardboard samples.....	19
6.1.2 Measurements of cellulose and cardboard samples	19
6.1.3 Measurements of anti-counterfeit markers.....	20
6.2 HECL studies.....	23
6.2.1 Preparation of the electrodes.....	23
6.2.2 HECL measurements.....	25
6.2.3 Immunoassays.....	26
7. Results and Discussion.....	28
7.1 Photoluminescence studies	28
7.1.1 Phosphorescence and fluorescence of cellulose materials.....	28

7.1.2	Multiple luminescence centres in cellulose.....	31
7.1.3	Cellulose materials as substrates for anticounterfeit markings	34
7.1.4	Authentication based on luminescence topography maps.....	35
7.2	HECL studies	41
7.2.1	Spin-coated polymer and composite films on metal electrodes	41
7.2.2	The effect of carbon particle content.....	44
7.2.3	The effect of free radical scavengers and co-reactants on HECL	47
7.2.4	Screen-printed electrodes	48
7.2.5	Analytical applicability of composite electrodes	51
8.	Conclusions.....	57
	References	59

List of Abbreviations and Symbols

AC	Anti-counterfeit
BA	Bioaffinity assay
AFM	Atomic force microscopy
BB	Baseboard with one layer of coating
BP	Birch cellulose
CAP	Cellulose acetate propionate
CB	Carbon black
CCD	Charge-coupled devices
CD	Carbon dots
CL	Chemiluminescence
CRP	C-reactive protein
CV	Cyclic voltammetry
EC	Ethyl cellulose
ECF	Elemental chlorine free
ECL	Electrochemiluminescence
ECLIA	Electrochemiluminoimmunoassay
EMCCD	Electron multiplying charge-coupled device
FITC	Fluorescein isothiocyanate
G	Graphite
HECL	Hot electron induced electrochemiluminescence
HNQ	Hydroxynaphthoquinone
HP	Hydrophobic
HSV	Hue, saturation, value

LF	Line/finger type of electrodes
LTM	Luminescence topography map
MFC	Microfibrillar cellulose
NFC	Nanofibrillar cellulose
OBA	Optical brightening agent
PL	Photoluminescence
PLP	Persistent luminescence phosphors
PS	Polystyrene
PUF	Physical unclonable functions
QR	Quick response
RGB	Red, green, blue
RS	Round-shaped electrode
RSD	Relative standard deviation
SB	Higher quality paperboard
SEM	Scanning electron microscope
Td	Delay time
Tg	Gate time
TEMPO	2,2,6,6-tetramethyl-1-piperidinyloxy
TR	Time-Resolved
YCbCr	Luma, chroma blue, chroma red
$\Delta\lambda_{\text{ex/em}}$	Excitation or emission slit
$\lambda_{\text{exc/em}}$	Excitation or emission wavelength
$W_{\text{g/cb}}$	Weight fraction of G or CB

List of Publications

This doctoral dissertation consists of a summary and of the following publications, which are referred to, in the text by their numerals:

1. Grönroos, P., Bessonoff, M., Salminen, K., Paltakari, J. & Kulmala, S. 2018. Phosphorescence and fluorescence of fibrillar cellulose films, *Nordic Pulp and Paper Research Journal*, 33, 246-255. <https://doi.org/10.1515/npprj-2018-3030>.
2. Salminen, K., Grönroos, P., Tuomi, S. & Kulmala, S. 2017. Cathodic electrogenerated chemiluminescence of aromatic Tb(III) chelates at polystyrene-graphite composite electrodes, *Analytica Chimica Acta*, 985, 54-60. <https://doi.org/10.1016/j.aca.2017.07.035>
3. Grönroos, P., Salminen, K., Paltakari, J., Zhang, Q., Wei, N., Kauppinen, E. & Kulmala, S. 2019. Hot electron-induced electrochemiluminescence at cellulose derivatives-based composite electrodes, *Journal of Electroanalytical Chemistry*, 833, 349-356. <https://doi.org/10.1016/j.jelechem.2018.12.006>
4. Grönroos, P., Nur-E-Habiba, Salminen, K., Nissinen, M., Tuomaala, T., Miikki, K., Zhang, Q., Wei, N., Kauppinen, E., Eskola, J., Härmä, H., Kulmala, S. 2019. Immunoassays Based on Hot Electron-Induced Electrochemiluminescence at Disposable Cell Chips with Printed Electrodes, *Sensors*, 19, 1-13. <https://doi.org/10.3390/s19122751>

Author's Contribution

Publication 1: Phosphorescence and fluorescence of fibrillar cellulose films

The author planned the experimental procedures and was responsible for all the spectroscopy measurement presented in the publication. The author wrote the manuscript of the article under the supervision of S.K. The production of fibrillar cellulose films was carried out by M.B. and J.P. Atomic force microscopy-imaging was performed by M.B. The manuscript was critically reviewed by J.P. and K.S.

Publication 2: Cathodic electrogenerated chemiluminescence of aromatic Tb(III) chelates at polystyrene-graphite composite electrodes

The author participated in the electrode manufacturing and performing the measurements with K.S., and in the writing process of the manuscript under supervision of S.K. Cyclic voltammetry experiments were performed by S.T. and sheet resistivity measurements by K.S. The manuscript was proofread by S.T.

Publication 3: Hot electron-induced electrochemiluminescence at cellulose derivatives-based composite electrodes

The author wrote the manuscript of the article under the supervision of S.K. The author planned the experimental procedures together with K.S. and performed all the luminescence experiments presented in the paper. Characterization of the electrodes by SEM and AFM was performed by Q.Z. and N.W. The manuscript was critically reviewed by J.P. and E.K.

Publication 4: Immunoassays Based on Hot Electron-Induced Electrochemiluminescence at Disposable Cell Chips with Printed Electrodes

The author wrote the manuscript of the article under the supervision of S.K. The author planned the experimental procedures together with N.-E.-H. and performed all the luminescence experiments presented in the paper. The design of the electrodes by K.S. and screen-printing of the electrodes by T.T. and M.N. Characterization of the electrodes by SEM and AFM was performed by Q.Z. and N.W. and by 3D surface profiling of electrodes and 2D surface analysis by N.-E.-H. Long-exposure photographs were taken and processed by K.M. Labelling and purification of labelled antibodies was performed by J.E. and by H.H. The manuscript was critically reviewed by N.-E.-H. and E.K.

1. Introduction

Luminescence is an emission of light that occurs when an excited state of atom or molecule relaxes radiatively to its ground state. In photoluminescence (PL) the excitation is produced by photons, whereas in hot electron-induced electrochemiluminescence (HECL) hot and/or hydrated electrons induce redox reactions, which lead to the excitation of luminophores. Luminescence methods can be utilized e.g. in research and development efforts for qualitative and quantitative analysis of luminescent substances, and in quality control to study the purity of the studied material or the changes occurring during the manufacturing process. Luminescence methods are also widely used in biochemical and biophysical applications such as immunoassays. [1] Due to the unique nature of luminescence phenomenon, and the high sensitivity, specificity and non-invasive character of luminescence detection methods, luminescent markers are also used in many kinds of anti-counterfeit (AC) technologies. [2–10]

Cellulose is a renewable material that can be used as a substrate in various luminescence applications. [11–16] In order to be able to utilize cellulose and nanofibrillar cellulose substrates in photoluminescence applications, their luminescence properties have to be understood. In this research work, the fluorescence and phosphorescence of solid cellulose samples were studied, and the possible sources of luminescence were considered. The influence of fibrillation method on luminescence properties was also investigated in this thesis. (Publication 1) In addition, the luminescence properties of cardboard materials were studied with the aim of adding AC markers on product packages.

An AC marking should have properties which make not only the replicating of the security label difficult, but also the knowledge of how the information can be utilized should be non-obvious. E.g. some parts of the information can be visible under UV-light with a naked eye, while some can be seen only from the instrumentally measured luminescence spectra. The possibility for portable detection is necessary in order to make such methods available also to the end users and not just research laboratories. The use of smartphones as luminescence detectors would make such techniques more accessible. The use of different luminescent markers and their detection methods for AC solutions are discussed in this thesis.

In HECL measurements, hot electrons are normally generated by pulse polarization of an electrode coated with a thin insulator layer. The insulating layer makes the tunnel emission of energetic electrons from the electrode to the solution possible [17–20]. Polymers such as polystyrene (PS) (Publications 2, 4) and cellulose derivatives (Publications 3, 4) have been studied as insulating materials in this work. Composite electrodes can be produced e.g. by spin-coating and by printing techniques using polymer containing carbon particles as an ink. The properties and performance of PS-graphite (PS-G) electrodes were first compared with more traditionally used oxide-covered aluminium electrodes (Publication 2). The possibility to replace PS with more environmentally friendly cellulose derivatives were studied next (Publication 3). PS and ethyl cellulose (EC)-carbon black (CB) composite materials were used in the fabrication of screen-printed electrode chips (Publication 4).

Some aromatic Tb(III) chelates exhibit high HECL emission intensity and a relatively long luminescence lifetime. This makes the use of electrode materials generating relatively high background emission, such as oxide-covered aluminium electrodes, possible when time-resolved detection is used. However, when the aim is to develop more inexpensive immunoassay methods, the use of low-cost luminescent labels with a short luminescence lifetime should be considered (Publication 4). The performance of screen-printed electrodes and the usability of fluorescein isothiocyanate (FITC) as a label were studied and compared to the results obtained with materials used in earlier studies. The immunoassays of C-reactive protein (CRP) were used to confirm the practical applicability of the method. (Publication 4)

In summary, the study and use of environmentally friendly materials (Publications 1, 3, 4), for the development of anti-counterfeit technologies (Thesis) and new materials for low-cost immunoassays (Publications 2, 3, 4) are all commercially valuable topics. This thesis compendium is organized so that the chapters 2, 3, 4 and 5 provide a brief introduction to the principles of luminescence, the development of luminescent labels, the luminescent properties of cellulose and hot electron electrochemistry, respectively. The experimental methods used in this research are presented in chapter 6 and the significant results obtained are discussed in chapter 7. Finally, the main conclusions of this research are summarized in chapter 8.

2. Principles of Luminescence

Luminescence is usually classified depending on the nature of the source of energy used for achieving the excited state. In photoluminescence (PL), the excitation is produced by photons and it can be further divided into fluorescence and phosphorescence according to the nature of the excited state. In chemiluminescence (CL) methods, the excitation energy is produced by chemical reactions. In electrochemiluminescence (ECL), at least one of the reactants resulting in the chemical reaction is produced electrochemically. In particular, during hot electron-induced electrochemiluminescence (HECL), hot and hydrated electrons generated at the electrodes induce redox reactions, which lead to the excitation of a luminophore. [21]

In both PL and HECL, the luminescence processes are similar after excitation, since both the redox reactions and photoexcitation result in the same excited states. However, both excitation methods have their own characteristics, benefits and limitations, which are discussed next.

2.1 Photoluminescence

Photoexcitation is possible using a light source with sufficiently high photon energy and intensity. Luminescence spectrometers typically consist of at least a light source, excitation and emission monochromators, sample holder and a detector, similar to conventional spectrophotometers. While in absorption spectrometry, the light absorbed by the sample is measured, in luminescence measurements only the emitted light is desired to be detected. In liquid samples, the cuvette is usually placed at a 90° angle to the light source, while with solid samples, the angle is selected so that the excitation light would not reflect towards the detector.

Excitation efficiency is an important parameter in luminescence, since the emission intensity is directly proportional to the excitation light intensity. Several types of light sources can be used as excitation sources: mercury and mercury-argon lamps, with lines from UV to IR; pulsed xenon lamps and xenon gas discharge lamps with emission at about 200-750 nm; and lasers, laser diodes and LEDs available in various wavelengths. [1] The use of LEDs and laser diodes is

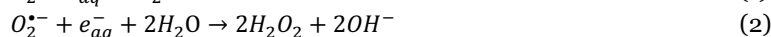
beneficial in portable and hand-held instruments due to their small size. Lasers emit a very narrow wavelength band of light, which makes the use of excitation monochromator or filter unnecessary, however the same excitation wavelength is often usable only for limited luminophores. When excitation sources with broader bandwidths are used, filters, slits, and mirrors play an essential role in providing sufficient resolution and the selection of the exact excitation wavelength. Filters can also be used to reduce the background emission caused e.g. by the matrix, or Raman and Rayleigh-Tyndall scattering. [1,22]

Photomultiplier tubes are the most commonly used detectors in traditional luminescence spectrometers. Charge-coupled devices (CCD) have also become common due to their relatively small size, easy connectivity, relatively high sensitivity, wide linear range, and relatively low cost. [1,22,23] With time-resolved (TR) detection, the signal-to-background ratio and sensitivity is better than in standard fluorescence measurements, [21] since e.g. in pulsed methods the excitation light is completely turned off and the background caused by scattering effects are eliminated. This simplifies the optics and lowers the cost of the equipment. [21,24] However, when the excitation has to be pulsed, this increases the requirements for the equipment.

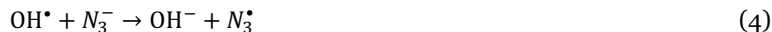
When small size and low-cost equipment with accurate and reliable detection are needed, some compromises must be made. When high wavelength resolutions are needed, the use of full sized laboratory equipment is necessary. However, even a smartphone can be used as a luminescence detector in many modern applications, when similar accuracy is not required. These topics are discussed in detail in this thesis.

2.2 Hot electron-induced electrochemiluminescence

In HECL, the excitation process is more complex than in photoluminescence. In HECL hot and hydrated electrons induce one-electron redox reactions, which lead to the excitation of luminophores. These high-energy electrons are normally generated upon the pulse polarization of an electrode coated with a thin insulator layer. [17] Electrons are first injected into the conduction band of water, then thermalized and subsequently hydrated, forming oxidizing radicals when reacting with dissolved oxygen or added co-reactants such as peroxodisulphate. [20] Since oxygen is usually present in the solutions, oxyradicals are generated by one-electron reduction (Equations 1-3 [20]):



An azidyl radical is rapidly produced when an azide ion reacts with a hydroxyl radical (Equation 4 [25]):



Peroxodisulphate produces highly oxidizing sulphate radicals at near diffusion controlled rate when hydrated electrons are present (Equation 5) [26]:



The simultaneous presence of both extremely strong one-electron oxidants and reductants allows difficult redox reactions to occur and enables the excitation of label compounds. [20] The excitation route is dependent on the lifetime and the redox properties of all the radical species involved in the system in an aqueous solution. Label luminophores can first be one-electron reduced by a presolvated hot or hydrated electron to a corresponding radical species (Equation 6). The formed luminophore anion radical is then one-electron oxidized back to its original oxidation state by a strong one-electron oxidant, leaving the luminophore in its excited state (Equation 7). [27]



Alternatively, the luminophore is first one-electron oxidized to a radical species (Equation 8) and then one-electron reduced by a hot presolvated electron or hydrated electron to its excited state. (Equation 9) [27]



The excited luminophore finally emits light, similarly as after photoexcitation.

The HECL instrumentation is relatively simple compared to PL, since excitation light and monochromators are not needed. The voltage needed for excitation is typically produced by a pulse generator, however even the use of direct current excitation is possible with certain electrode materials, if instrumentation is required to be simplified even further. A lightproof sample cell with cathode, anode and the sample holder is also relatively compact. Photomultiplier tubes are typically used as detectors, and gated photon counters make the TR measurements possible. However, all the similar detectors as in PL are usable when the emission intensity is sufficiently high.

Cathode material is one of the most important factors in HECL measurements, since the energy levels required for the generation of the hot electrons are not achievable using traditional electrode materials. Different electrode materials and their properties are discussed in detail in this thesis and in the Publications 2-4.

3. Luminescent labels and markers

Understanding the factors influencing the luminescence of organic compounds is important when new materials are investigated, or when the emission properties of the compounds e.g. markers or labels, are desired to be altered.

Luminescence of aromatic and other highly unsaturated aliphatic structures is typically caused by conjugated π systems, where an electron can be promoted from a π orbital to an antibonding π^* orbital ($S_0 \rightarrow S_n$). Transitions from n orbital to π^* may also produce weak emission from first excited singlet state S_1 . However, when the intersystem crossing becomes fast enough to compete with transitions from S_1 to S_0 , the process leads to emission from the triplet state T_1 . [1,22]

Emission from the triplet state occurs at longer wavelengths, and has longer lifetime due to the involved processes, where the excited electron has to reverse its spin before transition to T_1 , and again when returning to S_0 . [1,22] Transition metal–organic ligand complexes display mixed singlet–triplet states, since the spin multiplicity of the central ion may change or it may remain unchanged in an emissive process. [21]

Luminescent molecules are often sensitive to changes in their environment. Not only the concentration of luminophore, but also temperature, polarity and pH, and various quenching effects (e.g. by oxygen or heavy atoms) can have an effect on the luminescence intensity, quantum yield, emission maxima and luminescence lifetimes. At high luminophore concentrations, the proximity of fluorescent groups can cause an inner filter effect if their emission and absorption wavelengths overlap. [1,22]

The rigidity of the molecule reduces non-radiative transitions and intra-molecule vibrations and enhances luminescence. The chelation with metal ions stiffens the structure and enhances transitions to triplet state. [1]

The greater the extent of the π electron system, the lower the energy of π to π^* transitions, and consequently the absorption and emission spectra are shifted to longer wavelengths and the quantum yield is increased. Functional groups can also change the photophysical properties due to conformational changes.

For example, the carboxylic group can be in a position close to coplanarity of the ring structure, which induces an intramolecular charge-transfer character to the π - π^* transition. The electron donating groups (e.g. -OH, -OR, -NH₂, -NR₂) tend to increase the emission probability from the S₁ state, while electron withdrawing groups (e.g. -C=O, -COOH, -NO₂, -Cl) tend to decrease it and add the probability to long lifetime luminescence. Similarly, a heteroatom in a π conjugated system has an effect on the energies of n- π^* and π - π^* states and emission properties, often by decreasing the absorption coefficient and increasing the luminescence lifetime. [1,22]

The properties of different luminophores, luminescent matrixes and the applications of these materials are discussed next.

3.1 Organic luminophores and metal chelates

Organic luminophores such as fluorescein and its derivatives are used as probes and labels e.g. in bioaffinity assays due to their high quantum yield [21], and as spectroscopic markers e.g. in authentication, due to their low cost and easy availability [28]. However, fluorescein has a short Stokes shift, which lowers the signal-to-noise ratio, and it is relatively easily photobleachable. Fluorescein isothiocyanate (FITC) is one of the most important fluorescein derivative labels, and it is usable e.g. in immunoassays [24] due to the isothiocyanato group that is easily coupled with amino groups in protein and peptide chains [29,30]. Emission maximum of fluorescein is at 515 nm and that of FITC is at 522 nm. [31]

Organic molecules are often used as ligands to form chelates with metals, such as terbium(III), europium(III) or ruthenium(II). In case of lanthanides, the ligand works as an antenna and energy is transferred from the singlet state of the ligand through its triplet state to the resonance state of the metal.

Tris(bipyridine)ruthenium(II) chloride (Ru(bpy)₃²⁺) is currently the most widely used label in ECL. [32] However, it does not have similar importance as a label in HECL or photoluminescence applications, due to the better usability of other labels such as fluorescein and lanthanide(III) chelates in such applications. Ru(bpy)₃²⁺ emits light from its metal-to-ligand excited tripled state by a broad emission band with a maximum at 620 nm [33].

Terbium(III) and europium(III) ions form complexes with organic ligands, and can emit visible light with f-f transitions. [21] Figure 1 shows a simplified example of the electronic states, and the processes leading to emission from S₁ and T₁ states of the ligand, as well as the delayed luminescence from the resonance levels of a transition metal ion.

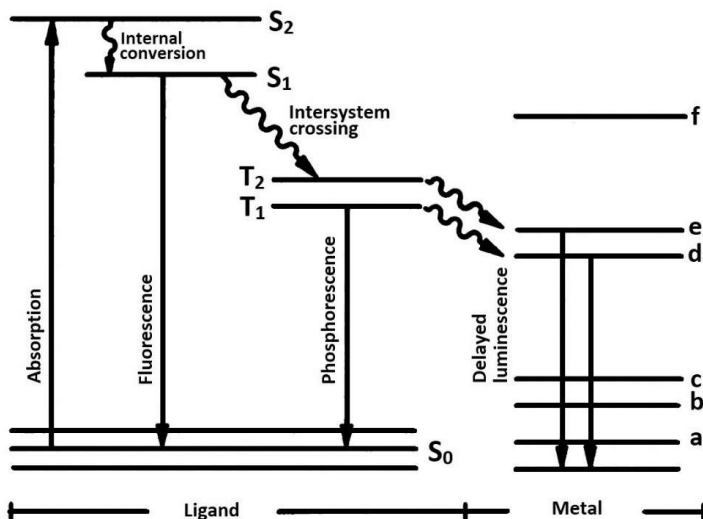


Figure 1. The electronic energy levels and transitions in a fluorescent organic molecule. S_0 = ground state, $S_{1,2}$ = excited singlet and $T_{1,2}$ = excited triplet states of the ligand. a-f = the resonance levels of the rare-earth ion. Straight arrows = radiative energy transfer, wavy arrows = nonradiative energy transfer. [24]

The emission peaks for Europium are due to the transitions ${}^5D_0 \rightarrow {}^7F_0$: 580 nm, ${}^5D_0 \rightarrow {}^7F_2$: 613 nm, and ${}^5D_0 \rightarrow {}^7F_4$: 690 nm, and for Terbium(III) ${}^5D_4 \rightarrow {}^7F_6$: 490 nm and ${}^5D_4 \rightarrow {}^7F_4$: 545 nm. [34] The 4f orbitals are shielded by the electrons in the 5s and 5p shells, so they do not participate in the formation of chemical bonds. Because of this, the effect of the matrix is small, causing sharp emission peaks at the same wavelength in solution. [35] However, especially in the solid state, matrixes have a significant effect on the excitation, and on the emission intensity and luminescence lifetime as discussed next.

3.2 Persistent luminescence phosphors

Persistent luminescence phosphors (PLP) are typically inorganic materials, consisting of a host lattice, doped with low concentration of metallic impurities called activators and sensitizers. In PLPs, the sensitizers absorb the energy and transfer it through the luminescent material to the activator, which is then responsible for the emission. The long decay time is due to the storage of the excitation energy by energy traps, and the gradual release from them with thermal energy. This phenomenon is often called as long lasting phosphorescence or even phosphorescence, even though the phenomenon is not due to triplet-to-singlet transitions, as in the case of phosphorescence of organic compounds. [36,37] The commercial PLPs were originally based on different sulphide materials such as ZnS doped with Cu^{2+} [38], and the luminescence lifetimes were up to few hours. With more recently developed alkaline earth aluminate phosphors, the emission intensities are higher and the lifetimes can be 25 hours and even

more. [37] The examples of commercially available rare earth co-doped PLPs' emission spectra are presented in Figure 2.

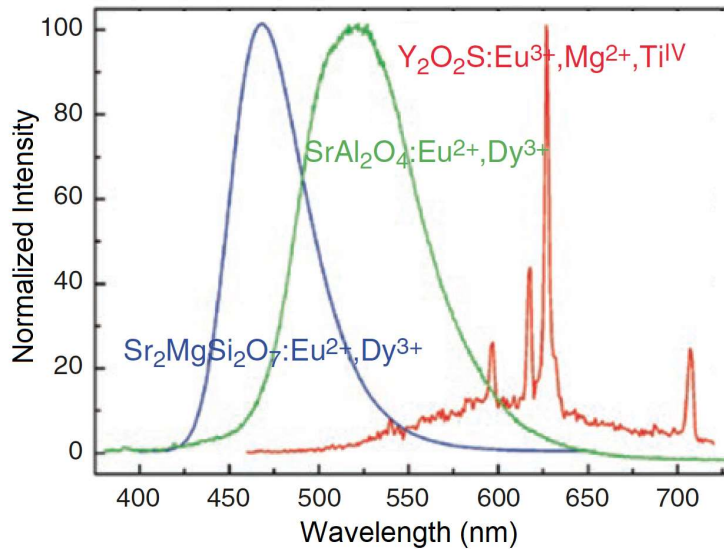


Figure 2. The luminescence emission spectra of blue, green and red emitting phosphors after UV excitation [37].

The emission colour can be adjusted by changing the absorbing and emitting impurity ions, and the afterglow can be shortened by adding some quenching impurities. [36] In addition, the properties of the host-lattice also have an effect on the luminescence. The mixed crystal proportions, e.g. in the ZnS–CdS–Cu system, have an effect on the electron traps, and at high CdS contents some relatively deep electron traps are produced [39], which have an effect on both emission maxima and luminescence lifetimes. [36]

The properties of the PLPs can be adjusted by multiple parameters depending on the application and the budget. Some host materials (both MA_2O_4 and $M_2MgSi_2O_7$, M: Ca and Sr) are otherwise rather inexpensive, however the high purity requirements increase their price. [37] Also ZnS based PLPs are still widely used in applications where highest emission intensities and lifetimes are not needed. Different PLPs are used in light sources, displays, detectors such as X-ray screens and scintillators, biomedical applications, and in track and trace and anti-counterfeit applications. [40,41]

3.3 Luminescent markers in anti-counterfeit applications

The range of counterfeit products is wide, and different product types require their own authenticity and traceability markings, depending on their size, material and intended use. Overt features, such as colour shifting inks, are visible with a naked eye. Semi-covert techniques, such as luminescent figures, are visible under UV-light. Covert techniques have information, e.g. from luminescent markers, which can only be read with an external reader. In forensic techniques, luminophores are present in trace amounts or their information is so difficult to analyse, that laboratory level testing is required. In track and trace techniques, products have some kind of unique code, which can be verified in every step of the products' supply chain. [42]

Organic luminophores have been used as AC markers due to their easy availability and low cost. However, these markers are easily recognised and acquired by counterfeiters, which results in the illegal reproduction of taggants by them.[2] Therefore, in AC techniques, the luminescent markers should be tunable so that the marking would be too difficult, expensive or time-consuming to be reproduced. Due to this, a wide range of different AC markers are used based e.g. on lanthanide chelates [3,4], organic-inorganic hybrid materials doped with lanthanide ions [5], lanthanide-doped zeolite [43], and lanthanide-doped nanocrystals [6]. Also e.g. upconversion nanocrystals [7], quantum dots [8], and carbon dots (CDs) [9,10] have great potential as AC markers due to their tunable lifetime and emission properties.

The use of luminescent markers in AC techniques are often best known from valuable papers, where markings can be seen already with the naked eye under UV-light, and the information obtained from the markers can be analysed further in a laboratory. With laboratory level spectrometers, even highly complicated emission information can be separated by emission intensity, wavelengths and luminescence lifetimes. Further, luminescence markers can be combined with a wide variety of different forensic materials e.g. physical, spectroscopic, chemical and DNA markers [28], to create highly secured AC technology.

When the goal is to obtain an AC technology that is usable in various steps of the product's supply chain, some compromises with the security level must be made. Due to the rapid development of smartphones and their cameras, the authentication of covert luminescent labels by the end users is becoming a more and more realistic goal. Smartphones can be used in luminescence detection since they have high computing power, high-resolution cameras, and they are small sized and inexpensive compared to a traditional sensor system. The easy connection to internet and databases makes them even more usable. [5] With regular smartphones, different emission wavelengths cannot be separated as accurately as with grating. However, by using different colour models, such as RGB (Red-Green-Blue), HSV (hue, saturation, value) and YCbCr (Luma, Chroma Blue, Chroma Red), emitting colours can be represented in a numerical form.

Regardless of the used technology, the smartphone AC application should be able to decode the luminescent information, compare it to the database, and provide a description of the authentication to the user, so that they can be ensured that the product is genuine. At the same time, the application should be easy to use, reliable and low-cost. [40]

4. Cellulose as a material in luminescence applications

4.1 Basics of cellulose

The interest in developing sustainable alternatives to oil-based products is constantly increasing. Cellulose is one of the most abundant organic compounds on the earth. It is typically produced from the lignocellulosic biomass, which consists of cellulose, hemicelluloses, lignin, extractives such as starch, pectins, sugars, aromatics and fatty acids, and inorganic compounds [44]. It is also possible to produce cellulose e.g. by bacterial process, to be able to get pure cellulose without any traces of the above-mentioned compounds.

Cellulose is composed of β -(1-4)-glycosidic linked glucose with three hydroxyl groups that cause cellulose to form hydrogen bond networks with the molecule itself, with other cellulose molecules, and with other substances in the matrix. Hydrogen bonding gives cellulose a multitude of partially crystalline fiber structures and morphologies. [45] Cellulose differs notably from widely used oil-based polymers e.g. polystyrene (PS), in which the repeating phenylethene unit does not have similar functionalization as celluloses.

Cellulose is sensitive to hydrolysis and oxidation of the chain, forming acetal groups, and its hydroxyl groups can be modified to form cellulose derivatives. [45] Especially, oxidation with 2,2,6,6-tetramethyl-1-piperidinyloxy (TEMPO) has drawn attention for promoting selective oxidation of the hydroxyl groups at C-6, to form aldehyde and then carboxylic groups in cellulose. When the hydroxyl groups have been oxidized, the strong hydrogen bonding decreases and the mechanical separation of cellulose to 3-5 nm fibers becomes easier. [46,47] The development of cellulose nanofibers have attracted significant interest in the last few decades due to their unique characteristics, such as their high aspect ratio and ability to form strong network structures.

Various celluloses, such as fully bleached kraft and sulphite pulps, Whatman filter paper, and algal and bacterial celluloses, have all been found to show a characteristic fluorescence [48], and regardless of its origin, cellulose has observable photoluminescence. Different emission wavelength maxima (between 420 and 495 nm) have been reported depending on used excitation wavelengths (between 285 nm and 360 nm) [49,50], and multiple different functional

groups, impurities, interactions and structural changes have been proposed to be responsible for the luminescence of cellulose. [49,51–53]

4.2 Applications of cellulose

Cellulose can be used as a platform for wide variety of applications due to its unique properties. Nanocelluloses and cellulose derivatives, and their composites with inorganic and organic substances, have been used in e.g. biological applications, water treatment, sensors, reinforcing agents, energy storage materials, and in many other kinds of functional materials. [54]

By converting some or all of the cellulose molecule's three hydroxylic groups to other groups, the material's properties such as solubility, hydrophilicity and strength can be changed significantly. Cellulose derivatives such as ethers e.g. ethyl cellulose (EC), where part of the hydroxyl groups on the glucose units have been converted to ethyl ether groups, and esters e.g. cellulose acetate propionate (CAP), which contains acetyl and propionyl groups, are used for coatings, laminates, optical films, sorption media, additives in building materials, pharmaceutical and cosmetic products etc. [45].

Cellulose can be used as an insulating material due to the lack of intrinsic free electrons and holes. However, metallic or semiconductive structures can be added to cellulose chains by chemical bonding. [55] Chemical stability, electrical conductivity, photo-catalytic activity, and photosensitivity can be altered by adding conductive material into a cellulose matrix [55,56]. Cellulose-based composites have been used e.g. in gas sensors, capacitive sensor, UV sensors, humidity sensors and strain sensors. [57]

Cellulose based materials have been widely used in chemical sensors and as tools for environmental applications in fluorescence sensing, i.e. for detection of biological analytes. In most of the designs, chromophores are immobilized in a polymer membrane displaying analyte-dependent optical properties that are usable in sensors. [11] Nitrocellulose in particular is very commonly used substrate material in rapid diagnostic tests utilizing the principle of immunochromatography. [58] The room temperature phosphorescence of cellulose derivative-heavy metal composites has led them to be regarded as candidates suitable for bioimaging, molecular sensing, optical devices, and other applications. [12]

Cellulose fibers [13] and biobased plastics made of cellulose hydrogels [14] have been used as a matrix for luminescent labels, without changing the mechanical properties of matrix significantly. Cellulose nanocrystal films have been functionalized with CdS quantum dots. [15] Tempo-oxidised nanofibrillar celluloses (NFC) have been bound with CdTe [16] to produce tunable emission from QDs. All these materials can also be used in anti-counterfeit purposes. [13–16]

Cellulose has great potential to be used in wide variety of applications. The photoluminescence properties of cellulose have been studied in Publication 1 and cellulose derivatives are investigated as an insulating material in HECL applications in Publications 3 and 4.

5. Electrode materials for hot electron electrochemistry

In HECL, energetic electrons are injected from the electrode to the conduction band of water. HECL intensity is dependent on the processes occurring inside the electrode and at the electrode surface, since if the electron injected/transferred does not have sufficient energy, it will not be able to induce the chemical reactions necessary for the excitation of the luminophores. Electrons injected into the conduction band of water are first delocalized, subsequently thermalized and finally hydrated. Hydrated electrons act as mediators in chemical reactions leading to the excitation of the luminophores.

5.1 Metal electrodes

The generation of hydrated electrons is complicated because of the narrow electrochemical window of the water. With typical metal electrodes, high cathodic potentials lead to vigorous hydrogen evolution as presented in Figure 3. For low voltages, higher than the decomposition potential of water U^d , water is decomposed into hydrogen and oxygen (A-B). When the voltage is increased, the current density also increases and a gas layer develops around the electrodes. The density of the bubbles and their mean radius increase with increasing current density (B-C). When the terminal voltage is increased above the critical voltage U^{crit} , the bubbles coalesce into a gas film around the working electrode. Bright light emission is observed in the film when electrical discharges occur between the tool electrode and the surrounding electrolyte (D-E). [59]

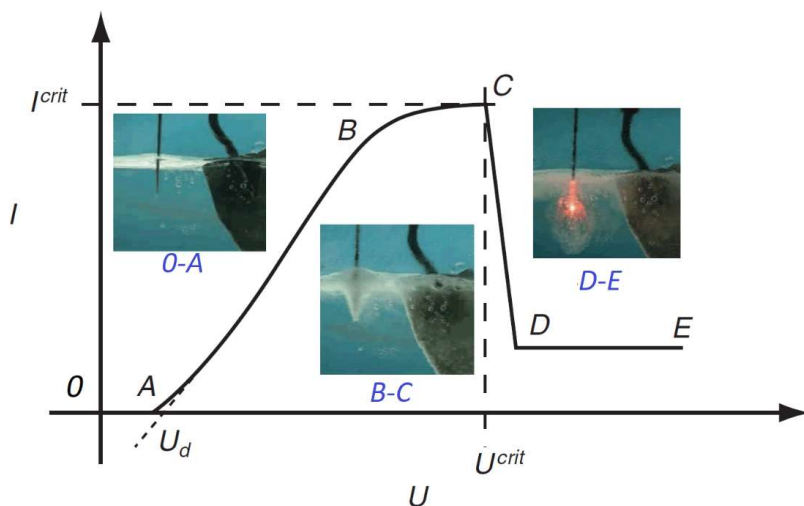


Figure 3 Typical current–voltage plot with photographs obtained around the tool electrode in 30% NaOH. [59]

Typical metal electrodes are not usable for generating hot electrons since i) the bright light emission causes too high background for the luminescent measurements, ii) the hydrogen generation is preferred over the generation of hydrated electrons [60], iii) the increase in electric current does not cause considerable change in the electrode potential, which is needed to generate hot electrons. These problems can be avoided by using electrodes covered with a thin insulating film.

5.2 Thin insulating film-coated electrodes

The insulating layer affects how the potential between the insulator covered metal electrode and the counter electrode changes as a function of externally applied voltage/current. The insulating film limits hydrogen generation at higher potentials and allows the transportation of kinetic hot electrons to the insulator/electrolyte-interface across the conduction band of the insulating film. [61]

HECL has been studied with several electrode materials coated with an insulating oxide layer (e.g. Al/Al₂O₃, Si/SiO₂, C/C_xO_{1-x} and Ta/Ta₂O₅) [20,62–64]. When electrons are tunnel emitted through an insulating film the thickness of the film greatly influences the HECL intensity. The optimal thickness of insulating layer in Al/Al₂O₃ electrode has been found to be ca. 2–5 nm. [20] If the film is thinner than 2 nm the injection of the electrons occurs before electron energy reaches the potential of the conduction band of water. With even lower film thicknesses, hydrogen formation is dominant and the potential cannot be raised to sufficiently negative values as described above [20]. If the insulating layer exceeds ca. 4–5 nm, Fowler–Nordheim tunneling starts to dominate as an electron transportation mechanism. Therefore, the layer has to be thin enough, so

that the direct field assisted tunneling of electrons is possible without the considerable loss of energy in scattering. [65]

Aluminum has a natural oxide layer coverage, with quite appropriate thickness of the insulating oxide film. This makes aluminium an easily producible and inexpensive material for HECL measurements. However, impure aluminium electrodes produce relatively high long-lived background emission, [66] and Al_2O_3 is known to be sensitive to pH due to dissolution of the insulating oxide layer [67]. Silicon does not have sufficiently thick natural oxide layer to produce good HECL efficiency. However, the oxide layer can be made thicker via e.g. thermal/anodic oxidation or atomic layer deposition [19,68]. Si/SiO₂ electrodes have shown excellent HECL performance in terms of low background luminescence in time-resolved measurements, electrode stability, and hydrated electron yield. However, the material and manufacturing costs of Si/SiO₂-electrodes are relatively high, especially when high reproducibility is required.

In addition to oxide films, HECL has been observed at oil film-covered carbon paste electrodes, where the electrodes were manufactured by simply pipetting paraffin oil onto the carbon paste electrode surfaces. [69] This demonstrates that thin insulating films can be produced by multiple ways. However, insulating organic polymer film covered electrodes have some drawbacks such as time-consuming manufacturing process, fragile nature of the polymer layer and the need for clean and expensive substrates. The background emission of electrode material during cathodic pulses can be caused by several parallel mechanisms, e.g. charge carrier recombination and excitation of luminescence centres in the insulating layer by hot-electrons, and emissions originating from the surface states of the insulating film at the solid/electrolyte interface [70]. This highlights the importance of the purity of the insulating material.

In composite electrodes, the insulating polymer material surrounds the conducting particles and enables electrons to be transported through the thin polymer layer to the electrolyte solution. The main advantage of composite electrodes over traditional insulating thin-film covered electrodes is their insensitivity to composite layer thickness and composition of the film [67,71,72]. Compared to oxide film-coated electrode materials, composite electrodes are found to have a more stable and reproducible HECL output in a wider pH range, and most importantly, without considerable background emission [72,73].

5.3 Applications of HECL in bioaffinity assays

HECL can be utilized in bioaffinity assays, e.g. in immunoassays. Immunoassays are based on strong binding between substances capable of stimulating an immune response (antigens) and proteins produced by the immunosystem in the response to antigens (antibodies).

In Figure 4, the principle of immunometric electrochemiluminoimmunoassays (ECLIA) is described. Capture antibodies are first physically attached to the insulating material of the working electrode. Then a sample solution, containing labelled antibodies and analyte, is dispensed on the electrode. The sandwich structure is formed when labeled antibody binds to antigen, which is already bound to capture antibody. The unbound labelled antibodies are washed away so that the measured HECL intensity is directly proportional to the amount of the analyte. Insulating film on the electrode surface works both as a solid substrate to immobilize the capture antibodies, and as the source of hot electrons capable of inducing the reactions needed for the excitation of the label luminophores.

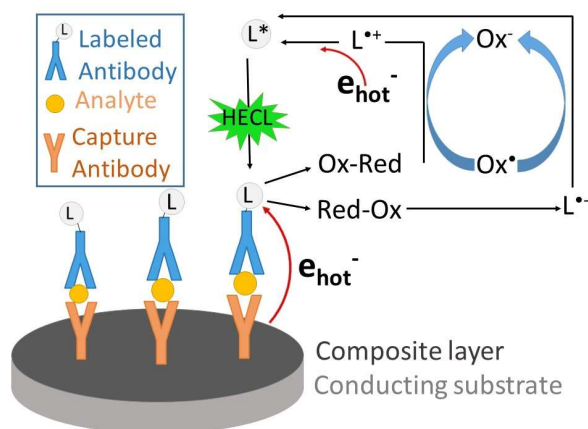


Figure 4. The principle of an electrochemiluminoimmunoassays. (Publication 3)

Tb(III) chelates have earlier been used as the main label in bioaffinity assays of C-reactive protein [20,72,74,75], β_2 -microglobulin [76] and human thyroid stimulating hormone [26,77,78], since they have relatively long luminescence lifetime, which enables time-resolved detection and thus the use of electrode materials generating relatively high background emission. However, when the electrode material is not producing high background emission during cathodic pulses, the use of low-cost luminophores with short luminescence lifetime, such as fluorescein isothiocyanate, opens up the possibilities to develop relatively inexpensive immunoassay protocols (Publication 4).

C-reactive protein (CRP) is a good point-of-care (POC) model analyte to demonstrate the feasibility of new electrodes and label materials in ECLIA, since it is regarded as an early indicator of infectious or inflammatory conditions, and as a universal biomarker for numerous diseases and disorders [79,80]. (Publication 3, 4)

6. Experimental

6.1 Photoluminescence studies

6.1.1 Fibrillar cellulose films and cardboard samples

Fibrillar cellulose samples used in this study were chosen to represent different fiber lengths and fibrillation methods. Samples were produced with a rapid method for production of fibrillar cellulose films [81]. Elemental chlorine free (ECF) bleached birch kraft pulp was chosen as the reference for birch cellulose (BP). Microfibrillar (MFC) and nanofibrillar celluloses (NFC) were prepared from the same bleached birch kraft pulp. For the first microfibrillar grade (MFC-1), the kraft pulp was first pre-refined to Schopper Riegler value 35 and then processed with MKZA10-15J Masuko grinder [82,83] for 4 passes. The second microfibrillar grade (MFC-2) was produced using a Microfluidics M-110P fluidizer with ten passes (200 μm and 100 μm chambers) without pretreatments [84–86]. And the NFC grade was prepared using TEMPO-oxidation and disintegration [87–89]. The oxidation step utilized chlorine dioxide (ClO_2) to activate the catalyst, and hypochlorite (OCl^-) to convert aldehydes to carboxylates. Films with target grammages of 40 g m^{-2} were produced from each cellulose grade.

Baseboard with one layer of coating (BB), and higher quality paperboard, with two coating layers (SB) (Metsä Board Oyj, Espoo, Finland), were chosen to represent different types of cardboard materials.

6.1.2 Measurements of cellulose and cardboard samples

(Publication 1)

Small pieces (1.5 cm \times 2.5 cm) of the different grades of cellulose films and cardboard samples were studied with a PerkinElmer LS50B luminescence spectrometer equipped with PerkinElmer front surface accessory 5212-3130. The sample was placed in a front-face set-up and the surface was at an angle of 35° with respect to the excitation beam. The irradiated area was 10 mm \times 3 mm.

Emission and excitation spectra, for determining emission maxima and standard deviations, were calculated from eight measurements made at different spots of the same sample from both sides. For each spot, 20 data points were

measured (around maxima, with intervals of 0.5 nm) which were then averaged. Average wavelengths and intensities at the maxima and their standard deviations were calculated from this data. Luminescence lifetimes were measured from only one sample spot, but the intensities at different delay times were also averaged from the 20 data points. Excitation wavelength used in the measurements was 286 nm. Emission wavelengths were set to 422 nm for fluorescence and 488 nm for phosphorescence excitation measurements. Emission slit ($\Delta\lambda_{em}$) was 20 nm wide and excitation slit ($\Delta\lambda_{ex}$) 15 nm wide. Emission filter 390 nm (long-pass) was used in the phosphorescence measurements.

The delay time (T_d) in phosphorescence measurements was 0.5 ms and in lifetime measurements from 0.1 ms up to 200 ms, and the gate interval (T_g) was 2 ms. Emission spectra in fluorescence and phosphorescence modes with different excitation wavelengths (240 nm to 400 nm) were measured under the same conditions as above.

Absorbance spectra (transmission light loss spectra) were measured with an Agilent 8453 UV-visible Spectroscopy System, with a deuterium-discharge lamp for the ultraviolet and a tungsten lamp for the visible wavelength range.

Atomic force microscopy-imaging was performed with Digital Instruments NanoScope Scanning Probe Microscope. Imaging was carried out in air, using a needle manufactured by Bruker. The frequency was 50–90 kHz, spring constant was 0.4 Nm^{-1} and scan rate was 0.977 Hz. Measurement software was ScanAsyst. Surface roughness of the scanned area was measured according to ISO 4287/1.

6.1.3 Measurements of anti-counterfeit markers

Markers were added on the cardboard samples analogous to AC markings on actual product packages. All the studied markers were unobtrusive and colourless in room light.

Luminescence topography map with luminescence spectrometer

The first series of measurements were made with the same PerkinElmer LS50B luminescence spectrometer as used in the measurements with cellulose samples. First a 100 μl volume of the marker stock solution containing $3 \cdot 10^{-5} \text{ mol l}^{-1}$ Fluorescein (Sigma-Aldrich) in water was added to a round area (1,77 cm^2) on the surface of the SB sample and allowed to dry. Emission spectra and standard curves were measured. Excitation wavelength (λ_{exc}) was 375 nm, emission wavelength (λ_{em}) was from 400 to 600 nm, emission slit ($\Delta\lambda_{em}$) was 5 nm and excitation slit ($\Delta\lambda_{exc}$) was 10 nm. Similarly, $10^{-5} \text{ mol l}^{-1}$ Terbium chelate (Tb(III)-L1) solution (ligand: 4-(3-aminobenzyl)-2,6-bis[N,N-bis(carboxymethyl)aminomethyl]phenol) was added on the surface of the SB and the luminescence was

measured using the parameters: $\lambda_{\text{exc}}=293$ nm, $\lambda_{\text{em}}=400\text{-}650$ nm, $\Delta\lambda_{\text{em}}=20$ nm, $\Delta\lambda_{\text{exc}}=15$ nm. $T_{\text{g}}=2.0$ ms, $T_{\text{d}}=0.2$ ms.

Next, the marker stock solutions of 10^{-4} mol l⁻¹ Tb(III)L1 and 10^{-4} mol l⁻¹ fluorescein in water were mixed together (1:1) and added on the surface of a BB sample and allowed to dry. A luminescence topography map (LTM) was measured using the parameters: $\lambda_{\text{exc}}=375$ nm, $\lambda_{\text{em}}=450\text{-}600$ nm, $\Delta\lambda_{\text{em}}=20$ nm, $\Delta\lambda_{\text{exc}}=15$ nm, $T_{\text{g}}=2.0$ ms, $T_{\text{d}}=0.1\text{-}5$ ms. In LTMs, the emission intensity as a function of emission wavelength and emission delay time was collected in the same database and expressed in a graphical form.

Luminescence topography map with charge-coupled device

Next, Andor Technology DV465C-FI electron multiplying charge-coupled device (EMCCD) detector attached to an Oriel Instruments MS125 (model 77400) spectrograph, equipped with a 100 μm slit and 300 mm⁻¹, 500 nm blaze angle grating, was used to measure LTM. Commercially available phosphorous inks from GloNation (Kentucky, USA) were used as markers. Neutral Orange glow powder and neutral Dark Blue glow powder were made to a 10 m-% water stock solution. This mixture was added on the surface of a BB sample and allowed to dry. A Nightsearcher UV LED flashlight (365 nm, 5W) was used as the excitation source, and switched off just before the measurement. Exposure time (t_{exp}) was 2 s and the number of kinetic cycles 200. The EMCCD was cooled to -63°C and the image was horizontally binned to obtain one-dimensional spectra of 560 pixels.

Luminescence topography map with smartphone camera

The third series of measurements were made to demonstrate the possibility of using smartphones in measuring RGB-based LTM. Super Glow Paint GloNation (Kentucky, USA) Blue, Green, Aqua, Dark Blue and White dyes were added on the surfaces of a BB sample and allowed to dry. The luminescence decay was measured by taking a series of photographs with Nokia Lumia 1020 smartphone at time intervals of 60 s. Nightsearcher UV LED flashlight ($\lambda=365$ nm, 5W) was used again for the excitation, and switched off just before the measurement. The RGB values and Brightnesses (in HSV system) were analysed using ImageJ Fiji software [90].

Product authentication technology with smartphones

The stock solutions were prepared from Neutral Orange glow powder (R) from GloNation (Kentucky, USA) and Green (G) and Blue (B) pigments from LumiNova® (NEMOTO CO. LTD, Tokyo, Japan). Each of the pigments was mixed with a transparent PVOH carrier to form stock solutions having 1 g of Red (O),

green (G) or blue (B) pigments in 10 ml of 25 m-% PVOH solution in H₂O. Eight unique taggants and their replicates, were created using these stock solutions as described in Table 1. The numbers in the table indicate how many times 50 μ l of each stock solution was added to the BB cardboard surface.

Table 1. The numbers indicate how many times 50 μ l of each stock solution was added to the cardboard surface.

Marker	Red (R)	Green (G)	Blue (B)
B	-	-	1
R	1	-	-
13BR	3	-	1
13GR	3	1	-
13BG	-	3	1
24BR	4	-	2
24GR	4	2	-
24BG	-	4	2

The markers were captured using Samsung S4 (version 4.4.2) and Lumia 1020 (version WP8.1) smartphones. The description of the measuring arrangement is shown in the Figure 5. The height of the camera module (extension) was adjusted accordingly to ensure that no image blur would be introduced, and the minimum focus distances of the S4 and the 1020 were determined to be around 100 mm and 150 mm, respectively. A light source (Yongnuo YN565EX external camera flash) was used to produce full-spectrum white light sufficient for the photoexcitation, and controlled by microcontroller/smartphone. The power and zoom level of the flash were set to 1/32 and 24 mm, respectively.

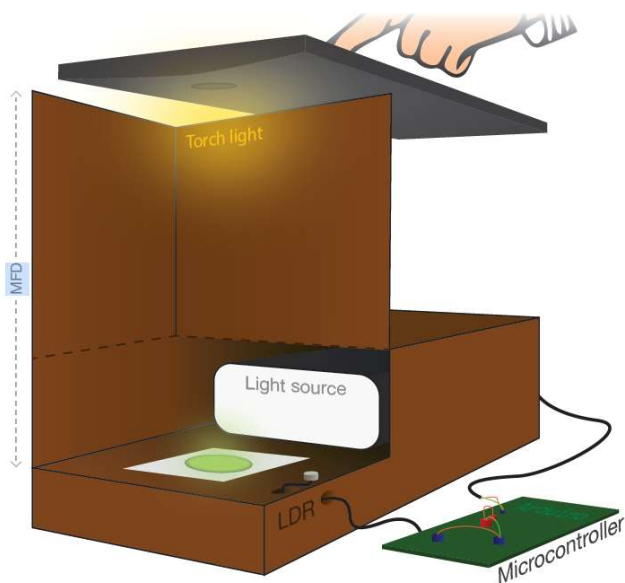


Figure 5. The camera module consists of an external light source, a Light-Dependent Resistor (LDR), and a microcontroller encased in cardboard. [91]

Six different capture presettings for the Samsung S4 (Android) and three different capture presettings for the Lumia 1020 (Windows Phone) were created. The presettings define a set of camera configuration parameters to be used for the fingerprint capture. All of the 16 markers (Figure 6) were captured with each of the presettings, resulting in a corpus of 144 fingerprints.

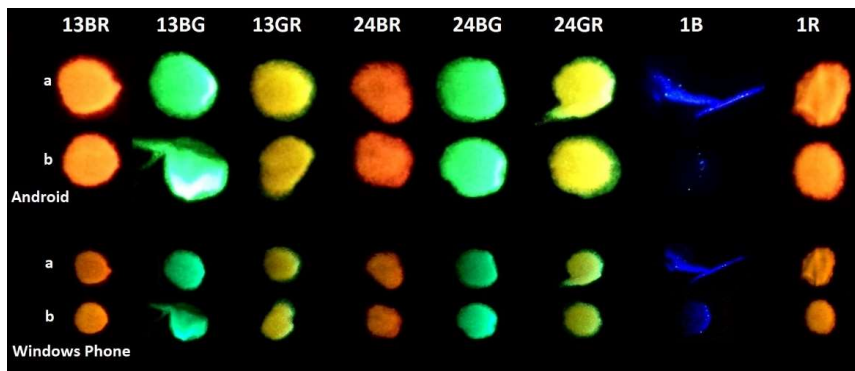


Figure 6. Captured marker samples with replicates a and b for both the Samsung S4 (top two rows) and the Lumia 1020 (bottom two rows). The brightness and contrast of markers has been increased for demonstration purposes.

In the peak finding process, each frame first went through a colour space conversion, where the pixel data was converted from the native YCbCr format to RGB, and then to HSV. The analysis algorithm utilizes the OpenCV (<http://opencv.org/>) open source computer vision library (version 2.4.9) for most of its computations. The parameters and algorithms are described more in detail elsewhere [91].

6.2 HECL studies

6.2.1 Preparation of the electrodes

Spin-coated polystyrene-graphite electrodes (Publication 2)

Polystyrene (PS, SKU 441147) was dissolved overnight in analytical grade chloroform at 50 g l^{-1} concentration. Graphite (G) flakes were then added in various weight ratios and the resulting solutions were mixed at 13 000 RPM (T-10 homogenizer, IKA) for one hour to ensure homogenous, aggregate-free dispersion. Freshly dispersed suspensions were spin-coated onto 0.05 mm thick brass substrates (15 mm in diameter). Spin-coating deposition was performed in normal room atmosphere at 3500 RPM for 60 s.

Spin-coated cellulose derivative-carbon black electrodes (Publication 3)

Cellulose acetate propionate (CAP, SKU 340642), Cellulose acetate butyrate (CAB, SKU 419052) and ethyl cellulose (EC, SKU 247499) were purchased from Sigma-Aldrich, and carbon black (CB, Vulcan XC72) from Cabot. CAP and CAB solutions were made in acetone and EC solution in toluene. The solutions were mixed with Cole-Parmer ultrasonic homogenizer (amplitude 20%, 500 W, 20 kHz). For spin-coating of the composite electrodes, the combined mass concentration of cellulose (CAP, CAB or EC) and CB was kept at 50 g l⁻¹ in all of the abovementioned cases. Cellulose materials and carbon black were mixed in various weight ratios. Also cellulose derivatives without CB were tested as insulating layers. Because of the high viscosity, the EC-solution's mass concentration was 5 g l⁻¹, whereas that of cellulose ester solutions were 25 g l⁻¹ for the cellulose-only spin-coating solutions. Cellulose layers were spin-coated onto steel (\varnothing = 15 mm) substrate in normal laboratory atmosphere. Flat aluminum sheets (Merck Art.101057, batch 721 K4164557, 99.9% pure) were used as a reference material without any pretreatments. Spin-coating was carried out using a WS-650MZ-23NPPB spin-coater (Laurell Technologies Corporation).

The EC-CB and CAP-CB films were characterized by scanning electron microscope (SEM, Zeiss Sigma VP) at 1 kV and by atomic force microscopy (AFM, Veeco Dimension 3100) in tapping mode.

Screen-printed composite electrodes

The composite solution mixtures were prepared using PS (SKU 441147) and EC (SKU 247499) purchased from Sigma-Aldrich, and CB (Vulcan XC72) from Cabot. Polystyrene and ethyl cellulose-carbon black solutions were made in benzyl alcohol (Acros Organics) as its volatility properties are suitable for screen-printing. The total mass concentration for PS-CB was 270 g l⁻¹, where the amount of carbon black was 40%, and for EC-CB the values were 150 g l⁻¹ and 30%, respectively. The mass ratios of these solutions were chosen based on the needed viscosity for screen-printing. The solutions were mixed with Cole-Parmer ultrasonic homogenizer (amplitude 20%, 500 W, 20 kHz).

Two types of electrode geometries were studied and tested in printed cell chips. The first type were round-shaped electrodes (RS electrodes), and the second were line/finger type of electrodes (LF electrodes) in which working and counter electrode lines were adjacent through the whole cell area. The schematic pictures of the electrodes are presented in Figure 7. The composite film served as the working electrode, and a silver film as the counter electrode, with a hydrophobic ring for sample confinement.

First, a layer of silver (Asahi silver ink) was screen-printed on the polymer substrate (Valox FR1 film). Then the electrode sheet was annealed at 140 °C for 30 minutes. The first layer included the design of the counter electrode and also

provided electrical contact for the composite ink layer. Next, one composite layer was screen-printed using the respective mask, and the electrodes were cured at 120 °C for 30 minutes. Further, a second composite layer was then screen-printed on top of the first layer to ensure full coverage of the underlying contact silver (Ag) layer, and then again cured at 120 °C for 30 minutes. Finally the hydrophobic (HP) ring was screen-printed using a dielectric paste (D2070423P5, Gwent Electronic Materials Ltd.). The net hole size was 60 μm and the thickness of wires was 45 μm (UX90-45; 230 wires/inch).

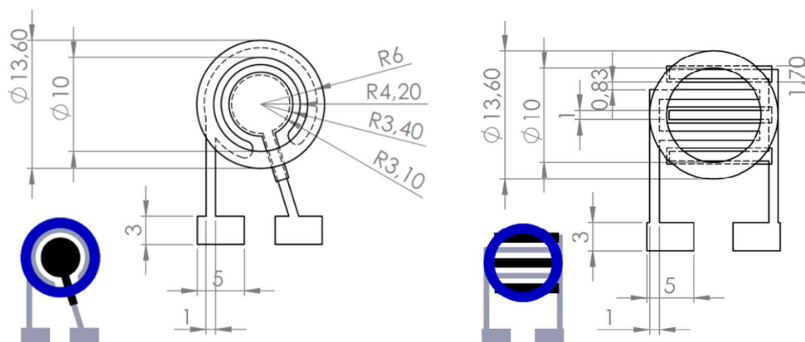


Figure 7. Schematic diagram of the screen-printed electrode chips RS (left) and LF electrodes (right). Anode was screen-printed with Ag ink (grey), cathode with EC-CB or PS-CB paste (black) on top of the Ag layer on working electrode areas and hydrophobic ring printed from dielectric paste (blue). Dimensions are given in mm. The cathode area (radius = 3.4 mm) of the RS is 46 % of the sample area ($r = 5$ mm) and in LF electrode it is 40 %. (Publication 4)

The EC-CB and PS-CB films were analysed by scanning electron microscope (SEM, Zeiss Sigma VP) at 1 kV in Aalto University Nanomicroscopy Center (Aalto-NMC) premises, and by atomic force microscopy (AFM, Veeco Dimension 3100) in tapping mode in Aalto NanoFab (Micronova).

Step height measurements of each layer on both EC and PS composite electrodes were analysed using Bruker Dekatak XTL stylus profiler at Micronova, Aalto University. Further topographical analysis of the surface was studied using optical profiler (Filmetrics Profilm 3D, Micronova, Aalto University).

6.2.2 HECL measurements

The HECL measurements with spin-coated composite electrodes or aluminium electrodes were made in a cylindrical Teflon cell ($\varnothing = 5.0$ mm), equipped with platinum wire counter electrode. The cell was screwed in contact with the electrode so that the distance between the electrodes was approximately 1 mm. In screen-printed electrodes, the working electrode, counter electrode and the sample confinement region were all integrated in the same chip.

The excitation pulses were generated with an in-laboratory-built coulometric pulse generator [20] or with a simple DC voltage supply. The constant charge

voltage, rate and electrical charge of the pulses are described in detail in Publications 2-4. A photomultiplier tube module (PerkinElmer MH1993, 1364-H-064) was used for the optical detection. The same (550 ± 20 nm) optical filter was used for Tb(III) chelates and fluorescein. With fluorescein, the slightly off-centered 550 nm optical filter allowed larger flux of photons to enter the photomultiplier tube than our 515 ± 10 nm filter and was therefore used in the measurements. Two channel gated SR400 photon counter with a DC-300 MHz amplifier (both from Stanford Research System) was connected to the photomultiplier along with a Nucleus MCS-II multiscale card. HECL emission spectra were also measured with Andor Technology DV465C-FI electron multiplying charge-coupled device (EMCCD) attached to an Oriel Instruments MS125 (model 77400) spectrograph.

Long exposure time photographs of HECL were taken in a completely dark room with Canon EOS 7D digital camera equipped with Canon EF 100mmf/2.8 L Macro IS USM lens. The camera and coulstatic pulse generator were turned on simultaneously. (Publications 2 and 4)

Tb(III) chelate Tb(III)-L2 (Publication 2) where the ligand was 4-(Phenylethyl)(1-hydroxybenzene)-[2,6-pyridinediylbis(methylene nitrilo)]tetrakis(acetic acid) and Tb(III)-L3 (Publications 3 and 4) where the ligand was 4-(Isothio-syanatophenylethyl) (1-hydroxybenzene)-2,6-diyl)bis-(methylenenitrilo)tetrakis(acetic acid) were obtained from Turku University. Ru(bpy)₃²⁺ and Fluorescein were obtained from Sigma-Aldrich. (Publication 3) All the HECL measurements were carried out in 0.05 M Na₂B₄O₇ buffer, at pH 9.2 with 0.1 M Na₂SO₄ as the supporting electrolyte.

6.2.3 Immunoassays

The working electrode was coated with primary anti-human CRP antibodies (anti-hCRP clone 6405, Medix Biochemica) via physical adsorption by dispensing 50 μ l of 5 μ g ml⁻¹ coating solution containing 50 mM Trizma base, 0.9% NaCl and 0.05% NaN₃ (pH 7.7). The coating reaction was carried out overnight (> 12 h). After the coating process, the electrodes were carefully dried with tissue paper. 50 μ l of a saturation solution containing 6% D sorbitol and 0.1% bovine serum albumin in TSA buffer (50 mM Tris, 0.05% NaN₃, 0.9% NaCl, pH 7.7) was dispensed on the electrode surface. Following the saturation phase (3 h), the electrodes were dried and washed three times with 100 μ l of 0.05 M Na₂B₄O₇, 0.01 M NaN₃, 0.1 M Na₂SO₄ solution, whose pH was adjusted to 7.9 using H₂SO₄. The heterogeneous immunoassays at electrodes coated with the primary antibodies were prepared by adding a mixture of human CRP (Scripps) and FITC (Publication 4) or Tb(III)-L4 (Publications 3 and 4), where the ligand was 1 (p-isothiocyanatobenzyl)-diethylenetriamine N¹,N¹,N²,N³,N³-pentaacetic acid (AD0029, PerkinElmer), with labeled secondary antibodies (anti-hCRP clone 6404, Medix Biochemica) diluted in DELFIA assay buffer (PerkinElmer).

The labeling of secondary antibodies was performed overnight at room temperature with a seventyfold excess of FITC or the Tb(III)-L4 chelate in 0.5 M sodium carbonate at pH 9, and the excess labels were removed via gel filtration (NAP-10 column containing Sephadex G-25, Pharmacia) with similar TSA buffer as above. Buffer exchanges were done with NAP-5 column containing Sephadex G-25 (Pharmacia). hCRP samples were made by diluting the stock solution of hCRP solution with TSA buffer containing 0.5% BSA, 3.5 mM CaCl₂, 0.05% bovine γ -globulin and 0.01% Tween 20 (pH 7.7). 15 μ l of labeled antibody solution was dispersed evenly over the electrode surface. The electrodes were then washed similarly as in coating and saturating phases. The amount of FITC or Tb(III)-L4 labelled secondary antibodies was 100 ng per electrode. All saturation and coating procedures were carried out in a closed humidior that had aqueous azide solution at the bottom to provide necessary vapour pressure.

7. Results and Discussion

7.1 Photoluminescence studies

The goal of these photoluminescence studies was to find a cellulose based material with as low as possible background luminescence, so that it could be used as a substrate for anticounterfeit luminescent markers displaying low luminescence intensities. Materials with background luminescence caused by wood constituents or even optical brightening agents can be used as substrates if their luminescence does not interfere with the measurement. The background luminescence of fibrillary cellulose films, birch pulp films, recycled plain carton and higher quality paperboard, as well as different marking strategies with selected luminophores and substrate materials, and possible authentication methods were studied in this work.

7.1.1 Phosphorescence and fluorescence of cellulose materials

The most interesting material for low background luminescence applications was found to be TEMPO oxidated NFC, which has more careful fibrillation process, and therefore less potential luminescent wood constituents, such as hemicellulose, proteins, pectin and lignin, compared to other studied microfibrillar cellulose types (MFC-1, MFC-2).

The photoluminescence properties of fibrillary cellulose samples were compared to that of BP (Publication 1). Baseboard with one layer of coating, and higher quality paperboard, with two coating layers, were also studied to gain information about the possible similarities with photoluminescence of the fibrillary samples, and to examine the background luminescence of these potential substrate materials.

Absorbance spectra of the studied materials were first measured and only NFC had a clear absorption maximum (at 250 nm), while possible maxima of the other fibrillary cellulose samples were covered in high transmission light losses caused by light scattering. In addition to NFC being the most translucent and having finer fibers compared to other samples, it probably has functional groups

formed during the oxidation and fibrillation processes, such as carboxylates, which absorb light. (Publication 1)

Information about the luminescence excitation maxima is needed when the possible emitting groups are investigated, and when luminescent markers are added to the substrate, so that unwanted background luminescence can be minimised by choosing suitable excitation conditions. Examples of each sample type's fluorescence and phosphorescence emission and excitation spectra are presented in Figure 8.

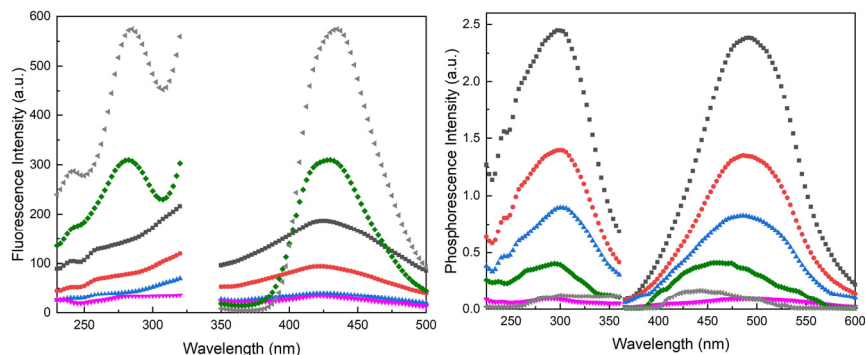


Figure 8. Fluorescence excitation ($\lambda_{em}=422$ nm) and emission ($\lambda_{exc}=286$ nm) spectra, $\Delta\lambda_{em}=20$ nm, $\Delta\lambda_{exc}=15$ nm (left). Phosphorescence excitation ($\lambda_{em}=488$ nm) and emission ($\lambda_{exc}=286$ nm) spectra, $\Delta\lambda_{em}=20$ nm, $\Delta\lambda_{exc}=15$ nm, $T_g=2.0$ ms, $T_d=0.5$ ms (right). ●: MFC-1, ■: MFC-2, ▲: BP, ▼: NFC (Publication 1), ◀: SB, ◆: BB.

All the studied materials had observable fluorescence and phosphorescence emission as can be seen from Figure 8. Fluorescence excitation maxima for BP, MFC-2 and MFC-1 were situated at around 260 nm. NFC, BB and SB had excitation maxima at 286.5 nm, 282 nm and 285 nm, respectively, which were close to the used excitation wavelength of 286 nm. NFC intensity did not increase after 300 nm as strongly as with other samples. The difference in excitation spectra of NFC sample again indicates that there are different types of emission centres present in comparison to those of the other samples.

The maximum luminescence intensities and the wavelengths at maximum intensities are presented in Table 2. The averages of the intensities and wavelengths of fibrillar celluloses and BP were calculated from eight replicate measurements (Publication 1), while the information of SB and BB are from the data represented in Figure 8.

Table 2. Wavelength and standard deviation (n=8) at average max intensity (nm), and average intensity (a.u.) and standard deviation (n=8) of wavelength at max intensity (a.u.), $\lambda_{exc}=293$ nm.

Luminescence	MFC-1	MFC-2	BP	NFC	BB	SB
Wavelength at max. fluor. intensity (nm).	422 ± 1.5	424 ± 1.1	424 ± 1.1	421 ± 0.7	429	435
Average fluorescence intensity (AU)	80 ± 43	149 ± 104	43 ± 12	45 ± 31	310	580
Wavelength at max. phosp. intensity (nm),	488 ± 2.9	491 ± 2.5	486 ± 2.6	495 ± 3.4	460	443
Average phosphorescence intensity (AU)	1.5 ± 0.6	2.4 ± 1.3	0.9 ± 0.2	0.1 ± 0.05	0.4	0.2

Emission maxima shown in Table 2 were in agreement with the values found in literature. Cellulose has been found to have a broad fluorescence emission maximum around 420–460 nm [49], and phosphorescence emission maximum at 495 nm [50]. NFC fluorescence emission maxima was at shorter wavelengths and phosphorescence maxima was at longer wavelengths, compared to other fibrillary cellulose samples. The fluorescence maxima of cardboard samples were also at longer wavelengths compared to cellulose samples, which is expected since the main source of fluorescence in SB samples is from optical brightening agents (OBA) (maxima at around 440 nm [92]), whereas the BB-sample's emission is probably from a mixture of cellulose materials and OBA's emission.

The phosphorescence emission intensities of MFC-1, MFC-2 and BP samples were of the same order of magnitude as their fluorescence emission intensities. However, NFC, SB and BB phosphorescence emission intensities were decreased notably, which indicates that the optical brightening agents used in the cardboard samples, and changes induced in NFCs by TEMPO oxidation, favor fluorescence over phosphorescence. The fluorescence intensity of all fibrillary samples compared to BP were relatively high. The intensity of BP could have been expected to be higher due to possible traces of e.g. lignin. However, this is in agreement with the studies claiming lignin to be an insignificant source of luminescence in cellulose samples [49].

TEMPO-oxidation is known to add carboxyl content [87], and the presence of carboxylic groups in the anhydroglucose units has been found to shift the emission maxima to shorter wavelengths (blue-shift) and simultaneously increase their fluorescence intensity [93]. In this study, the emission intensity from NFC was not especially high, but the emission maximum was notably shifted to shorter wavelengths compared to that of the other grades, which again points out the NFC differences compared to other materials.

The high standard deviation of the intensities is indicative of the heterogeneity of the samples. This might be due to aggregates formed while producing a film. Especially, TEMPO-oxidized particles are known to have a tendency to form aggregates with significantly larger size, which might have an effect on the luminescence.

7.1.2 Multiple luminescence centres in cellulose

The possibility of cellulose having multiple luminescence centres has been known for a long time. Gavrilov and Ermolenko, who studied photoluminescence of cellulose with different excitation wavelengths, found three emission maxima in the regions of 370, 430-470 and 505-510 nm. They suggested that this was due to the cellulose having three different types of emission centres. [94] This was investigated in the current work by measuring the fluorescence and phosphorescence emission spectra with altered excitation wavelengths, and the luminescence lifetimes of the cellulose samples (Figure 9).

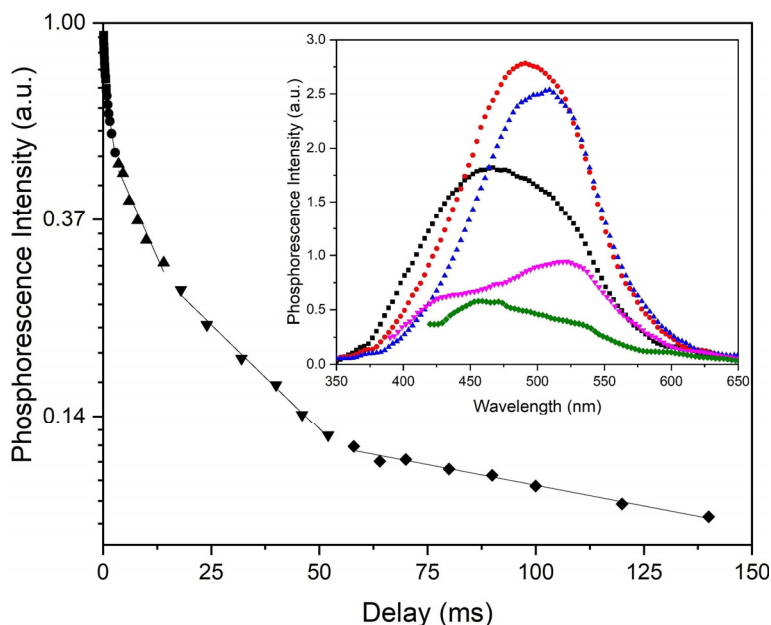


Figure 9. Phosphorescence decay curve of MFC-2 ($\lambda_{exc}=286$ nm), ($\lambda_{em}=480-490$ nm, average of intensity). $\Delta\lambda_{em}=20$ nm, $\Delta\lambda_{exc}=15$ nm, $T_g=2.0$ ms, $T_d=0.1-140$ ms. Inset: Phosphorescence emission spectra of MFC-2 with excitation at ■: 240 nm, ●: 280 nm, ▲: 320 nm, ▼: 360 nm, ◆: 400 nm. $\Delta\lambda_{em}=20$ nm, $\Delta\lambda_{exc}=15$ nm, $T_g=2.0$ ms, $T_d=0.5$ ms. (Publication 1)

The presence of multiple emission maxima and the multi-exponential phosphorescence decay confirms that there are several luminescence centres in the studied cellulose types. Especially in MFC-2 spectra, it is evident that the emission maximum changes from 466 nm to 530 nm when the excitation wavelength is altered from 240 to 400 nm. NFC seems to behave in the same way as MFC-2 but the emission intensity was so low that the noise makes interpretation of the

spectra less certain. At 610 nm ($\lambda_{exc}=400$ nm) there was one observable difference in NFC compared to MFC-2 which could indicate different emissive groups. (Publication 1)

In fluorescence spectra, the scattered excitation light is in the same wavelength region as the emission maximum, which makes interpretation of spectra more difficult. Emission maximum of all the samples were centred around 425 nm, however in NFC there appears to be a new emission maximum at 445 nm ($\lambda_{exc}=320$ nm) and at 480 nm ($\lambda_{exc}=360$ nm). (Publication 1)

Typical cellulose processing conditions (e.g. hot alkali) can induce the formation of small amounts of aromatic structures from reducing end groups or hemicelluloses [95]. Many of the structures identified in these studies are quinones [48]. Most of the primary chromophores belong to hydroxy-[1,4]-benzoquinones, hydroxy-[1,4]-naphthoquinones (HNQ), and hydroxyacetophenones [96–99]. The emission behaviours of MFC-2 and NFC samples were similar to those found for HNQ solution in cyclohexane, which emits at 400-500 nm and around 600 nm ($\lambda_{exc}=265$ nm), 400-500 nm ($\lambda_{exc}=380$ nm) and 550-700 nm ($\lambda_{exc}=460$ nm) [100]. However according to Zwirchmayr et al., oxidatively damaged cellulose chains produce HNQs [101], so higher emission intensity could be expected in the spectra of NFC, if the source of emission is HNQ. However, this was not observed (Figure 8), and the subject needs further studies in order to determine the exact origin of cellulose luminescence.

With cardboard samples, some changes in the emission wavelength and emission intensity as a function of the excitation wavelength were observed, however, these changes were more subtle compared to cellulose samples. The strongest fluorescence emission was observed with excitation wavelength at 375 nm, and the highest phosphorescence emission was with excitation wavelength at around 285 nm, similar to cellulose samples.

Luminescence decay curves of the MFC-2 (Figure 9), MFC-1 and BP were fitted to five separate lifetime components, which is equivalent to five independent decay processes, and NFC luminescence decay was fitted to four separate lifetimes (Table 3) (Publication 1). The lifetimes were fitted between selected delay times to make the comparison of the decay processes of these materials easier. The luminescent lifetimes of SB and BB were not measured, however when the decrease of luminescence intensity of all the sample types at delays of 0.1 and 10 ms were compared, the intensity of MFC-1, MFC-2, BP and BB decreased to 35-40 %, NFC to 10 % and SB to 1 %, which again indicates differences between the luminescent groups of these samples. Especially, OBA in SB favours fluorescence over phosphorescence, which is important to know when luminescent markers are added on cardboard.

Table 3. Luminescence lifetimes (τ) of BP, MFC-1, MFC-2 and NFC samples ($\lambda_{exc}=286$ nm), ($\lambda_{em}=480-490$ nm, average of intensity). (Publication 1)

Delay (ms)	τ MFC-2 (ms)	τ MFC-1 (ms)	τ BP (ms)	τ NFC (ms)
0.12-0.74	2.4	3.1	2.4	1.2
0.9-2.8	6.8	7.9	7.8	6.2
3.6-14.0	20.1	21.4	20.4	28.1
18.0-52.0	46.9	47.8	54.4	45.0
58.0-140	239.2	227.8	361.0	

Luminescence lifetimes show that BP had slower and NFC had faster decay than in other cellulose samples. NFC not only had lower phosphorescence intensity but its phosphorescence also seems to decay faster than that of other grades. One possible source for the observed luminescence has been suggested to be the transition metals left on the cellulose samples after normal preparation procedures [53]. The luminescence lifetime of Mn(II) emission, occurring at a wavelength range of 490 to 750 nm, is typically in the millisecond range [102], which is similar to the values obtained in the present study.

Although all the above mentioned functional groups, possible sources of contamination, as well as the formations of new luminescent structures during the pulping processes, have an influence on the luminescence of different celluloses, the effects of physical properties of cellulose have attracted interest in recent years. Crystallization is known to lock and rigidify the molecular structure, and together with the isolation from the quenchers, it has been found to boost the phosphorescence emission of pure organic luminogens [103,104] such as cellulose. Clustering of the chromophores with π and lone paired n electrons and subsequent overlapping of the electron cloud have also been stated to be responsible for the luminescence emission. [105] Aggregation-induced emission occurs in some polymers when aggregation restricts the intramolecular rotations, blocking the non-radiative pathway and opening up the radiative channel. [106] These findings are part of the growing interest towards nonconventional luminogens, free of aromatic groups, producing room temperature phosphorescence. The phenomenon has been attributed to multiple different polymer materials, not only for cellulose, which suggests that the origin of luminescence, or at least strongly enhancing effect on luminescence, might be in the physical and not just the chemical structures.

The results obtained with the fibrillary cellulose films studied in this work cannot be directly generalized to other fibrillary cellulose materials since the main goal of the fabrication technique here was to be rapid, and not to produce as pure and repeatable films as possible. However, the fluorescence and phosphorescence emission and lifetime measurements are clearly useful tools not only for the study of luminescent groups in cellulose, but also in quality control of

the film homogeneity, and in understanding effects of the different pulping conditions.

It is clear that cellulose luminescence emission does exist, and that there are differences in luminescence properties of the studied cellulose and cardboard samples. The actual origin of cellulose luminescence is far from unambiguous. Various chemical characteristics e.g. hydroxynaphthoquinones, metal ions forming complexes, and possible luminescence quenching and enhancing functional groups such as carboxyl and carbonyl groups, as well as the physical characteristics such as crystallinity, should be taken into consideration when the luminescence properties are studied. The effect of chemicals used in the oxidation should also be studied carefully, especially when the fibrillated cellulose films are desired to be used in luminescence applications.

7.1.3 Cellulose materials as substrates for anticounterfeit markings

For anticounterfeit markings, luminophore solutions were dried on SB and BB substrates to simulate the printing of labels on e.g. pharmaceutical packages. The emission spectrum and blank-corrected calibration curve for fluorescein, on the surface of SB cardboard, are represented in Figure 10.

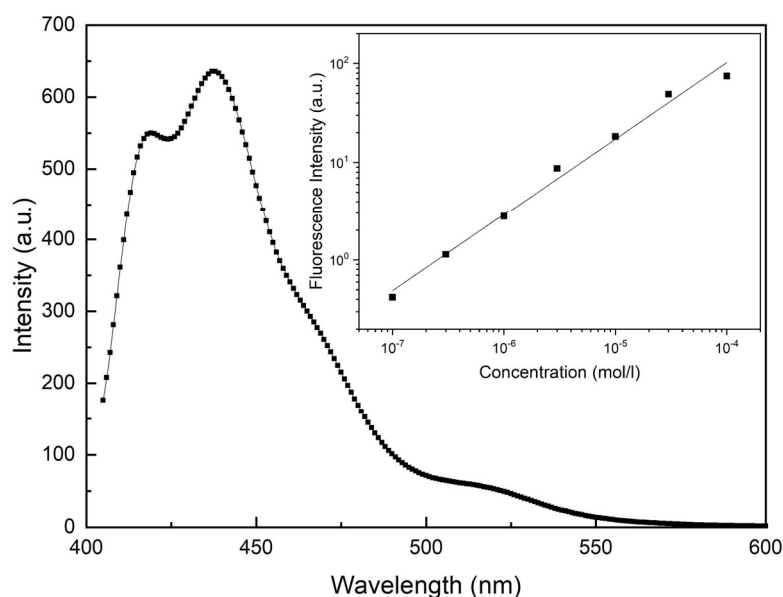


Figure 10. Emission spectrum of fluorescein 1.7 nmol cm^{-2} ($=3 \cdot 10^{-5} \text{ mol l}^{-1}$ solution) on the surface of SB cardboard displaying strong background luminescence. Inset: Calibration curve. Average emission intensity at $\lambda_{\text{em}}=520\text{-}522 \text{ nm}$. $\lambda_{\text{exc}}=375 \text{ nm}$, $\Delta\lambda_{\text{em}}=5 \text{ nm}$, $\Delta\lambda_{\text{exc}}=10 \text{ nm}$. Linear area $5.65 \text{ pmol cm}^{-2}$ – $5.65 \text{ nmol cm}^{-2}$.

As can be seen from Figure 10, the emission of fluorescein at relatively low concentration levels was only weakly observable due to the strong background emission from the cardboard substrate. An excitation wavelength of 375 nm was used to enable emission from both fluorescein and OBA, so that the emission of

fluorescein would not be noticeable with the naked eye under typical hand-held UV-lamps. However, the calibration curve for fluorescein was linear over three orders of magnitude of concentration. With BB as a substrate, background luminescence would have been lower and linear area could have been wider. However, this is a more realistic situation when real product packages are used.

Emission spectrum and calibration curve of Tb(III)-L1 were similarly measured but in time-resolved mode (Figure 11).

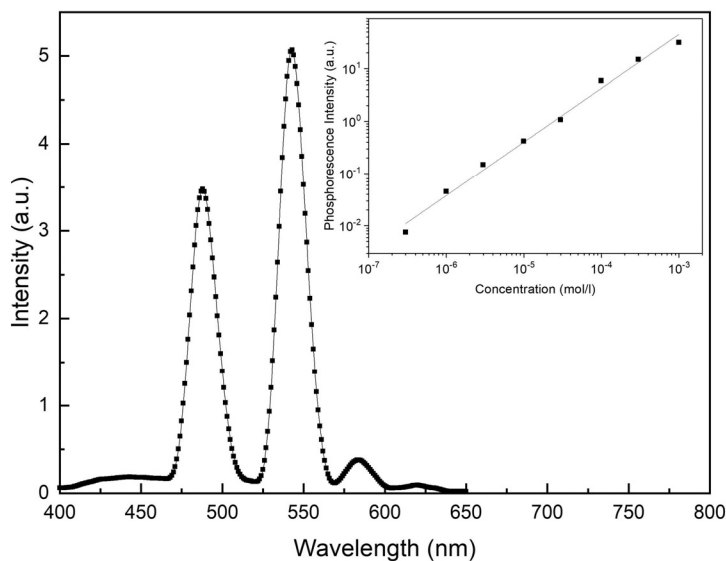


Figure 11. Phosphorescence emission spectrum, $5.65 \text{ nmol cm}^{-2}$ ($=10^{-4} \text{ mol l}^{-1}$ solution) Tb(III)-L1 on SB cardboard. $\lambda_{\text{exc}}=293 \text{ nm}$, $\Delta\lambda_{\text{em}}=20 \text{ nm}$, $\Delta\lambda_{\text{exc}}=15 \text{ nm}$. $T_g=2.0 \text{ ms}$, $T_d=0.2 \text{ ms}$. Inset: Calibration curve Tb(III)-L1 on SB cardboard, $\lambda_{\text{exc}}=293 \text{ nm}$, $\lambda_{\text{em}}=542.5 \text{ nm}$, $T_g=2.0 \text{ ms}$, $T_d=0.2 \text{ ms}$, $\Delta\lambda_{\text{em}}=20 \text{ nm}$; $\Delta\lambda_{\text{exc}}=15 \text{ nm}$. Linear area $16.9 \text{ pmol cm}^{-2} - 56.5 \text{ nmol cm}^{-2}$.

As discussed earlier, SB does not show long-lived luminescence. This can also be seen from the phosphorescence spectrum (Figure 11) where the emission of optical brightening agents is not significantly observable. This is important in the interest of packaging design, because product packages can keep their attractive appearance with optical brightening agents. Calibration curve was linear over almost four orders of magnitude. These results are promising for authentication markings on real product packages.

7.1.4 Authentication based on luminescence topography maps

Almost any kind of unique fingerprint can be used for authentication if the measurement data can be processed and analysed reliably and easily enough. In our luminescence topography maps (LTM), emission intensity as a function of emission wavelength and delay time is collected in one dataset and saved into the database. Measurement of full spectra with a large number of delay times is

not necessary for the recognition. It is sufficient to measure emission intensities with the most characteristic wavelengths and delay times, and compare these to the database.

Multiple combinations of different organic luminophores, lanthanide chelates and inorganic phosphors were studied and some examples are presented below. First, a mixture of fluorescein and Tb(III)-L1 markers were measured with laboratory level equipment to represent high security level authentication method. Then commercially available PLP inks were measured with CCD camera attached to a spectrograph. Finally, luminescence emissions of commercially available phosphors were detected with a smartphone camera to represent an authentication method for the end-users.

Figure 12 shows a luminescence map where a 1:1 mixture of fluorescein and Tb(III)-L1 has been dried on BB substrate.

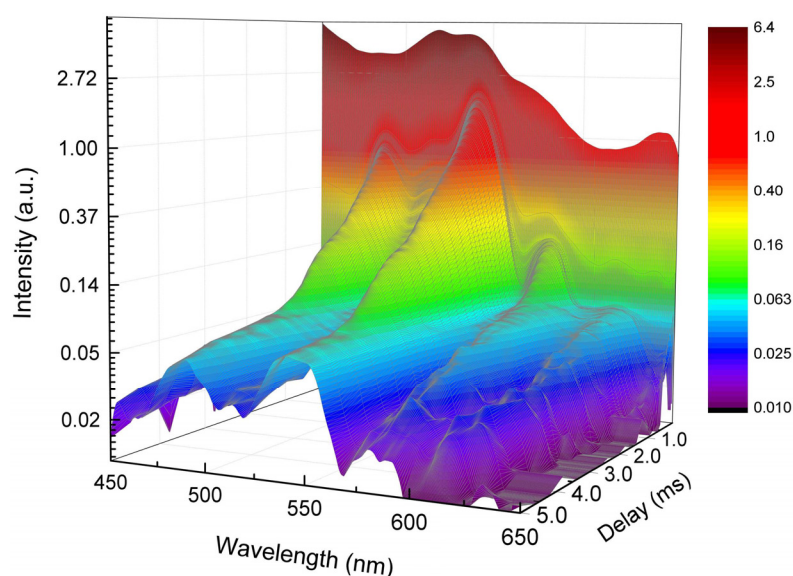


Figure 12. LTM of Fluorescein and Tb(III)-L1 1:1 mixture. $\lambda_{exc}=375$ nm, $\lambda_{em}=450-650$ nm, $\Delta\lambda_{em}=20$ nm, $\Delta\lambda_{exc}=15$ nm, $t_g=2.0$ ms, $t_d=0.1-5$ ms. Measured with PerkinElmer luminescence spectrometer.

As seen from the Figure 12, at the delay time of 0.03 ms, fluorescein's emission (max around 521 nm) and the fluorescence of optical brightening agents (highest at 450 nm) are still strong due to the tail of the excitation flash lamp, and Tb(III) chelate's emission is summed with these emissions. After the fluorescence emission has decayed, the terbium emission (at around 490 nm, 545 nm, 583 nm and 622 nm) is observable, and after Tb(III) chelate emission has decayed, the long lifetime phosphorescence of cardboard is observed. The luminescence of the substrate can also be used as part of a fingerprint, and as an inner standard, comparable to other parts of the package.

This kind of complex data should be analysed and compared to a database with a software developed for this purpose. Heavy data processing can be avoided if only selected parts of the data are used to calculate a value, which can be compared to a corresponding value in a database. A simplified example of this is represented in Table 4. When intensities at chosen wavelengths (450 nm, 460 nm, 521 nm and 545 nm), are compared at delay times of $t_1=0.01$ and $t_2=4.0$ ms, the characteristic decay relation ($r_d: I_{t_1}/I_{t_2}$) can be calculated. When decay relations at 450 nm and 460 nm are compared, the ratio ($r_r: r_{d450nm}/r_{d460nm}$) gives information also about the background intensity. At selected 4 ms delay time, short-lived luminescence from the marker luminophores has been decayed and long-lived emission from BB is observed. Based on the results discussed in chapter 7.1.2, BB can be expected to have emission still after tenths of milliseconds. However, when selecting time moments for calculations, it is important that not too long delay times are selected, in order to prevent obtaining insufficient signal-to-noise ratio. After the same ratio is calculated for decay ratios at 521 nm and 545 nm, the characteristic ratio for fluorescein and terbium is obtained. Finally, when these ratios (r_r) are compared the characteristic ratio (r_R) of the whole luminophore mixture is obtained.

Table 4. Fluorescein and Tb(III)L1 1:1 mixture. Intensities at selected wavelengths and delay times, and their ratios.

Wave-length nm	Delay t_{11} : 0.01 ms	Delay t_{12} : 4 ms	Decay ratio r_d : I_{t_1}/I_{t_2}	Ratio (r_r): $r_{d(\lambda_1)}/r_{d(\lambda_2)}$	Ratio (r_R): $r_{r(\lambda_1/2)}/r_{r(\lambda_3/4)}$
λ_1 : 450	6.34	0.022	287.7	1.2	0.54
λ_2 : 460	5.72	0.025	233.2		
λ_3 : 521	5.69	0.036	159.5	2.3	
λ_4 : 545	5.02	0.072	70.1		

The same can be expressed as an equation:

$$r_R = \frac{I_{\lambda_1 t_1} I_{\lambda_2 t_2} I_{\lambda_3 t_2} I_{\lambda_4 t_1}}{I_{\lambda_1 t_2} I_{\lambda_2 t_1} I_{\lambda_3 t_1} I_{\lambda_4 t_2}} \quad (10)$$

As seen from Table 4, the decay ratios r_d are characteristic for the used luminophores on the substrate. The lower the value of r_d , the longer the luminescence lifetime. Already these values give information if the cardboard material and luminophores are what they should be. The final value r_R can be compared with known reference value for the actual authentication of the product. However, before that, the wear and tear of the markings and proper error limits should be defined.

Luminescence topographic maps can be measured, and the relation values can be calculated, also from commercially available luminophores with simpler detection setup. PLPs were used to demonstrate this, and the phosphorescent

markings were made with a 1:1 mixture of GloNation Orange and Dark blue dyes, excited with UV led flashlight, and measured with EMCCD camera attached to a spectrograph. The obtained LTM is presented in Figure 13.

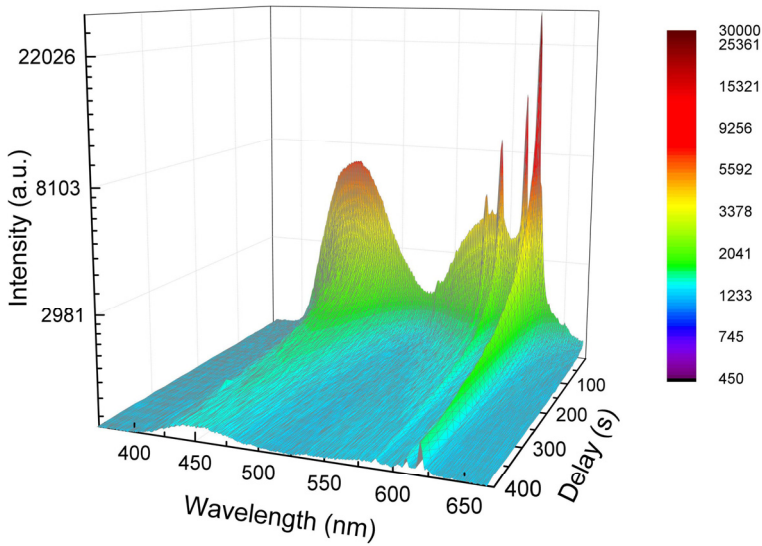


Figure 13. LTM of GloNation Orange and Dark Blue. Measured with Andor EMCCD-detector. $\lambda_{exc}=365$ nm, $t_{exp}=2$ s. Frame rate 0.5 fps.

Various emission maxima and lifetimes make the LTM usable for authentication. The data can be analysed similarly as before, with Equation 10. When the intensities at wavelengths 454 nm, 541 nm, 612 nm and 622 nm are compared at delay times of $t_1=1$ s and $t_2=200$ s, the characteristic decay relation is again obtained:

$$r_R = \frac{I_{\lambda_{454nm}t_2s} I_{\lambda_{541nm}t_{200s}} I_{\lambda_{612nm}t_{200s}} I_{\lambda_{622nm}t_2s}}{I_{\lambda_{454nm}t_{200s}} I_{\lambda_{541nm}t_2s} I_{\lambda_{612nm}t_2s} I_{\lambda_{622nm}t_{200s}}} = 4.3$$

In addition to spectroscopic techniques, various RGB readers, and RGB and HSV values can be utilized in authentication of the luminescent markings. This possibility minimises the costs of the detector, when the diffraction gratings and filters are not needed. To test this feasibility, commercially available PLPs were dispensed on different areas of BB cardboard surface, which could represent e.g. a part of the product logo or other figures in product package. The dots were let to dry, and the decay of their emission were recorded with a smart phone camera, after the excitation with a camera flash. A sequence of photographs were taken using Nokia Lumia 1020 camera phone with time intervals of 60 s. The pictures are presented in Figure 14.

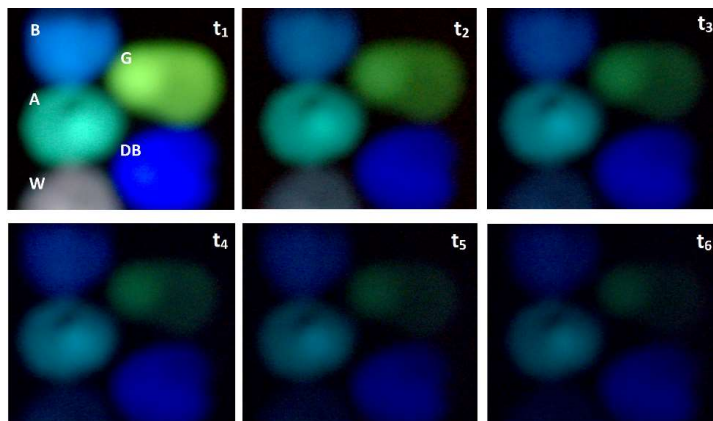


Figure 14. A sequence of photographs taken with a Nokia Lumia 1020 smartphone with time intervals of 60 s. Super Glow Paint Glonation (Kentucky, USA) Blue (B), Green (G), Aqua (A), Dark Blue (DB) and White (W).

From Figure 14, it can be seen already with the naked eye that the luminescence of some inks decayed faster than others, and the colours changed when decaying. The RGB values and Brightness (in HSV system) were analysed with ImageJ Fiji software [90] from the area where the studied ink was applied. As an example, the values of Glonation White at t_1 (0 sec) and t_6 (300 sec), and their relations are presented in Table 5.

Table 5. Glonation White at t_1 : 0 sec and t_6 : 300 sec. The RGB values and Brightness (in HSV system) were analysed with ImageJ Fiji software [90], and their relations were calculated.

White	t_1 : 0 s	t_6 : 300 s	Decay ratio $r_d: t_1/t_6$	Ratio (r_r)	Ratio (r_R)
Red	137.6	0.6	213.7	3.7	9.9
Green	138.6	2.4	58.2	0.4	
Blue	146.7	38.6	3.8		
Brightness	140.9	13.9	10.2		

All of the different spots could have been analysed similarly and different spots decays could have been compared to each other. However, already with the change of brightness values, the luminescence decay of different markers could be analysed. This kind of RGB analysing software could be made available as a smartphone application for the product's end users.

The smartphone application development work, part of a LuminoTrace project, was also carried out. The marker samples were designed and prepared by the author, while the designing of the fingerprint pipeline and the measurements were carried out by M. Raatikka with the details given elsewhere [91]. The principle of the developed method is represented in Figure 15. The studied markers were similar commercial PLP pigments as used above.

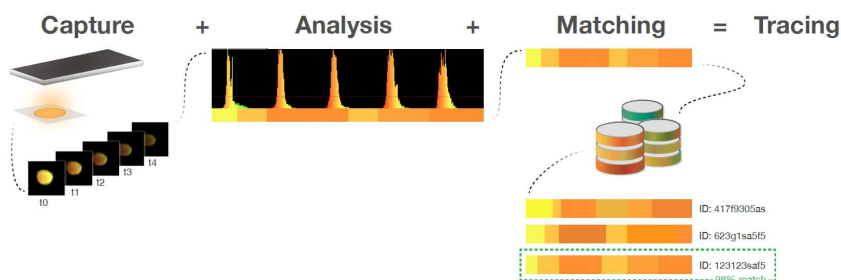


Figure 15. The fingerprint pipeline consists of capturing a marker, analysing it for a fingerprint and finding the best match from the database [91].

Samples were first excited with a camera flash, and after a delay, the selected number of frames were captured with smartphone camera, at set intervals. The analysis algorithm used the hue histogram of a captured frame as the basis for the analysis. For each frame, the algorithm finds the most dominant hues. The array of hue peaks were computed from all the frames to form a unique fingerprint. In the presettings, e.g. focus distance, torch resolution and interval (ms) were altered. Eight marker samples and their replicates were captured with six different presettings for the Samsung S4 and three presettings for the Lumia 1020, resulting in a database of 144 fingerprints. In the fingerprint matching step, the fingerprint was compared to the database to find the best match. The similarities were computed using the fingerprint matching algorithm and a more computationally intensive histogram method. The fingerprint's ability to match with its sibling fingerprint, i.e. to confirm product's authenticity, was 76 % with fingerprint method and 89 % with histogram method. Based on these results, the histogram presetting was more accurate. This accuracy is not yet enough to be used in real application. However, the results demonstrated possible ways to impliment an AC system, and gave valuable information about the challenges that need to be solved.

The luminophores were chosen to have long lifetimes so that a series of photos could be captured and analysed with a smartphone. However, the chosen colours were too similar, and the lifetimes were so long, that minor changes in the luminophore concentration and capture interval duration did not cause significant changes between the samples, which in turn caused recognitions to the wrong marker. Luminophores concentrations and emission colours should have been more distinguishable, and lifetimes of the marker should have been shorter, so that clear differences within emission intensities in the set delay time would have been noticed and the measurement time would have remained as short as possible, which is an important factor for the user experience. The marking preparation has a significant impact on fingerprint tracing, and the shapes, sizes and concentrations of sibling markings should be identical to be able to make reliable recognition with the used method.

At the moment, 960 frames per second (fps) is the highest rate for commercially available smartphones. If Tb(III) chelate with a lifetime of 1 ms (i.e. the emission

decays to $1/e$ in 1 ms) is used as a marker, and 5 frames are needed for the detection, the camera should be capable to take at least 5000 fps. Measuring low intensities also sets high requirements to the camera's aperture, shutter speed and ISO sensitivity. However, the results were promising especially since the camera technology and data processing capability of smartphones are constantly evolving and more secured markers (e.g. luminophores described in chapter 3) can be used.

Optical authentication system can be based on not only the use of RGB colour schemes, but it can be combined with almost any kind of overt, covert or forensic technique. For example, combining physical unclonable functions (PUFs), where random patterns of luminescent material are used, together with the luminescent information makes the duplication of individual labels even more difficult. [43] In many applications utilizing colour modes, luminescent markers have been combined with track and trace technologies to get more secured AC systems. In typical QR (Quick Response) codes, storage capacity and security can be improved by using a superimposition of the black-white and luminescent QR codes, utilizing RGB components produced by lanthanide based luminophores activated under UV light. [5,40]

The markings can be added to the surface of any product, as long as the matrix effects and the wear and tear can be taken into account. Cardboard was an interesting matrix due to its wide spread use in product packages, and the luminescence emission from constituent OBAs and celluloses can be used as a part of the authentication. OBA's strong emission can be deployed to hide the marker's lower emission, and also the option of using the long lifetime emission of cellulose gives new possibilities to the authentication.

7.2 HECL studies

The goal of these HECL studies was to find low-cost alternatives for expensive oxide-coated silicon electrodes. The possibility of using cellulose derivatives or PS films as insulating material on metal electrodes was tested first. Next, the composite electrodes made of different conductive carbon and insulating polymer materials were studied. (Publications 2, 3) Finally, these materials were used to make screen-printed electrode chips. (Publication 4) The analytical applicability of these electrodes was tested with immunoassay of CRP with a Tb(III) chelate label (Publications 3 and 4) and fluorescein derivative label (Publication 4).

7.2.1 Spin-coated polymer and composite films on metal electrodes

Steel substrate coated with thin layer of EC and CAP with mass concentrations of 5 g l^{-1} and 25 g l^{-1} , respectively, were studied first. Decay of the HECL emission

and time-resolved HECL of Tb(III)-L3 as a function of pulse ordinal are presented in Figure 16.

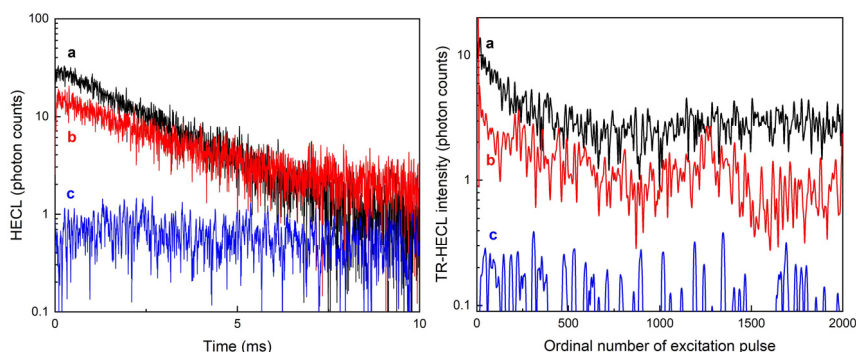


Figure 16. Decay of the HECL emission (left). TR-HECL as a function of the ordinal number of the excitation pulse. Delay 50 μ s and gate 1 ms. (right) 10^{-3} M Tb(III)-L3 in 10^{-3} M $K_2S_2O_8$, 0.05 M $Na_2B_4O_7$, 0.1 M Na_2SO_4 solution. Electrode materials: (a) steel with a thin layer of EC (b) steel with a thin layer of CAP, (c) steel without any insulating layer. Conditions: 2000 excitation pulses, pulse charge 9.0 μ C, voltage -35 V, frequency 50 Hz. Interference filter (550 ± 20 nm). (Publication 3)

The long-lived emission of Tb(III) chelate was obtained with cellulose derivative-coated electrodes, while with the bare metal substrates it was not observed. This proves that the insulating polymer film enables the tunnel emission of energetic electrons, and therefore electrochemiluminescent excitation of lumino-phore, during cathodic excitation pulses. The tested EC and CAP films tolerated at least 2000 excitation cycles without electric breakdown, which is promising because for an immunoassay already a tolerance of 200 excitation is normally sufficient. (Publication 3) When pure polystyrene with a mass concentration of 50 g l^{-1} was spin-coated onto brass substrate, no light emission from Tb(III) chelate was observed. (Publication 2) For a PS solution made with optimal mass concentration, the results would probably have been similar as with cellulose films. The optimization of the thickness of polymer layer in nanometer scale, and sufficiently reproducible manufacturing of the layers, was observed to be critically important for these results.

Due to difficult manufacturing process and low emission intensities, these electrodes were not studied further, and instead composite electrodes with different conductive carbon particles and insulating polymer matrixes were studied next. TR-HECL as a function of the ordinal of the excitation pulse and the decay of the background emission of oxide-covered aluminium, CAP-CB and EC-CB electrodes are presented in Figure 17.

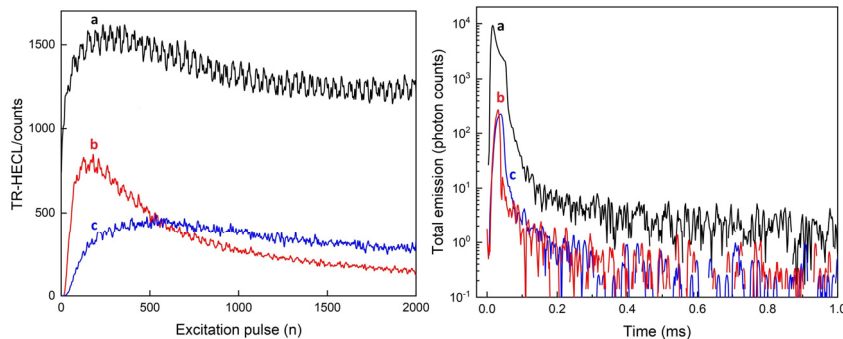


Figure 17. TR-HECL 10^{-5} M Tb(III)-L3 as a function of the ordinal of the excitation pulse. Delay 50 μ s and gate 1 ms (left). Decay of the background emission (right). Conditions: 0.05 M $\text{Na}_2\text{B}_4\text{O}_7$, 0.1 M Na_2SO_4 solution. Electrode materials: (a) Aluminum, (b) CAP-CB, (c) EC-CB, (W_{cb} 30%). Excitation: 2000 excitation pulses, pulse charge 9.0 μC , voltage -35 V, frequency 50 Hz, interference filter ($550 \pm 10\text{nm}$).

Compared to plain cellulose derivate films, the TR-HECL intensity of the composite electrodes (W_{cb} 30 %) was almost 100-fold higher even though the Tb (III)-L1 concentration was considerably lower. However, when the performance of CAP-CB and EC-CB electrodes (W_{cb} 30%) were compared to aluminium electrodes, TR-HECL of Tb(III)-L3 was only about 30 % of emission intensity obtained at oxide-covered aluminum electrodes. (Figure 17, left) This is at least partly due to carbon absorbing considerable amount of the HECL emission in the composite electrodes, whereas aluminum somewhat reflects it towards the detector. Similar results have been observed also with other composite materials. [71,72] However, the background emissions of EC-CB and CAP-CB electrodes were only about 2 % of the background emission observed from rather impure (99.9 %) aluminum electrodes, which indicates better S/N ratio than with aluminium electrodes.

The composite films tolerated several thousand excitation cycles in measurements without a breakdown. TR-HECL as a function of the ordinal of the excitation pulse with aluminium electrodes was high already after first pulses, while it took longer time to rise with composite electrodes. A similar effect was observed with PS-G electrodes. (Publication 2) When the PS-G electrodes were treated with sulphuric acid before the HECL measurement, the number of pulses needed to obtain highest emission intensity seemed to increase, possibly due to more exposed graphite particles present on the electrode surface. Further, the observed decrease in the emission intensity points out the importance of the insulating layer with such composite electrodes. It is possible that, when the polymer film is too thin, the uninsulated graphite particles on the surface can only produce hydrogen evolution but not HECL, and after some kind of surface passivation, i.e. formation of hydrogen, HECL generation becomes possible when the pulse-polarization is continued. (Publication 2)

With EC-CB electrodes, emission raised slowly but stayed stable for 2000 excitation pulses, while with CAP-CB electrodes emission increased and decreased

more rapidly. This indicates that there are notable differences between the insulating layers of these materials. The effect of carbon particle concentration in PS-G, EC-CB and CAP-CB electrodes, and the properties of the composite layers were studied next.

7.2.2 The effect of carbon particle content

The optimal carbon particle/polymer ratios for HECL applications were investigated by measuring TR-HECL of 10^{-5} M Tb(III) chelates with varied electrode compositions (Figure 18). The relationship between G or CB weight fraction ($W_{g/cb}$) and measured emission intensity, together with the relative standard deviation (RSD) of HECL signal, was studied with PS-G (Figure 18, left) and EC-CB and CAP-CB (Figure 18, right) electrodes. The sheet resistivity as a function of W_{cb} is also represented in Figure 18 (left).

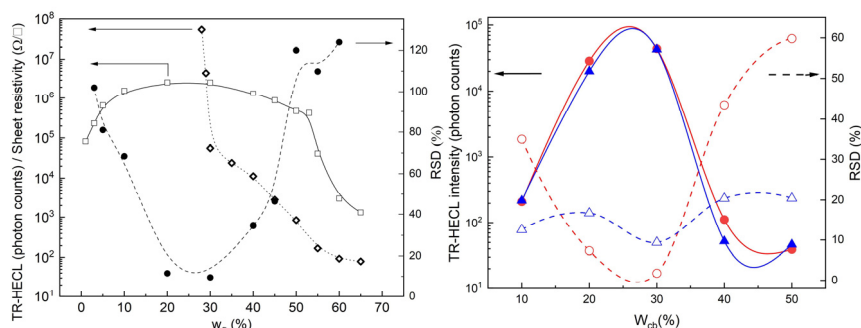


Figure 18. TR-HECL of 10^{-5} M Tb(III)-L2 at PS-G electrodes \square , as a function of G weigh fraction, the relative standard deviations (RSD) \bullet and sheet resistivity of electrodes \blacklozenge . Pulse charge 12.6 mC, frequency 20 Hz, delay 0, gate 4 ms. Interference filter (545 ± 20 nm). (left)(Publication 2) TR-HECL of 10^{-5} M Tb(III)-L3 at CAP-CB \bullet and EC-CB electrodes \blacktriangle as a function of CB weigh fraction and the relative standard deviations (RSD), CAP-CB \circ and EC-CB \triangle , 5 replicate electrodes. Pulse charge 9.0 μ C, frequency 50 Hz, delay 50 μ s and gate 1 ms. Interference filter (550 ± 20 nm). (right)(Publication 3) Conditions: 10^{-3} M $K_2S_2O_8$, 0.05 M $Na_2B_4O_7$, 0.1 M Na_2SO_4 solution. Excitation: voltage -35 V. 2000 excitation pulses

The electrodes were able to produce HECL at all tested CB weight fractions, however the highest intensities and the lowest relative standard deviations were observed for all electrode materials when W_{cb} was 20–30%. PS-G electrodes tolerated relatively great changes in the composition (W_g 10–50%) without major effect on emission intensity, while the HECL yield of CAP-CB and EC-CB electrodes decreased dramatically outside the W_{cb} range of 20–30%.

While the lower standard deviations were measured with CAP-CB electrodes, EC-CB electrodes results were more repeatable at all CB weight fractions. The standard deviation has to be as low as possible for analytical purposes. With this perspective CAP-CB could be used in the measurements. However, EC-CB was found to have better adhesion to the substrate, which is important in bioaffinity assays.

When approaching optimal conductive particle/insulating material composition ($W_{g/cb}$ 30%), HECL intensity rises since there are more carbon particles capable of generating hydrated electrons, and the average distance between the outermost carbon particles and the electrolyte solution decreases while the composite material's conductivity simultaneously increases. HECL intensity increases also when the optimal insulating film thickness is approached, and decreases again when the insulating layer gets too thin for tunnel emission of electrons to occur. Similar to oxide coated electrodes, where the HECL emission intensity has been shown to be highly dependent on the thickness of the insulating film [20,107], such effects have been observed with other carbon black composite electrodes as well [73].

The electron transport properties of composite materials are important for generation of hot electrons. The highest emission intensity and the lowest standard deviation was observed around the offset of coalescence network at approximately W_g 30%. The sheet resistance at this value was as large as $100 \text{ k}\Omega \square^{-1}$, which indicates that more conductive particles e.g. carbon black or carbon nanotubes should be used, especially if the composite layers are made thicker.

Cyclic voltammetry (CV) was used to analyse the surface of the glassy carbon/PS-G electrodes with varied compositions (Figure 19), i.e. to study the insulating film coverage further. (Publication 2)

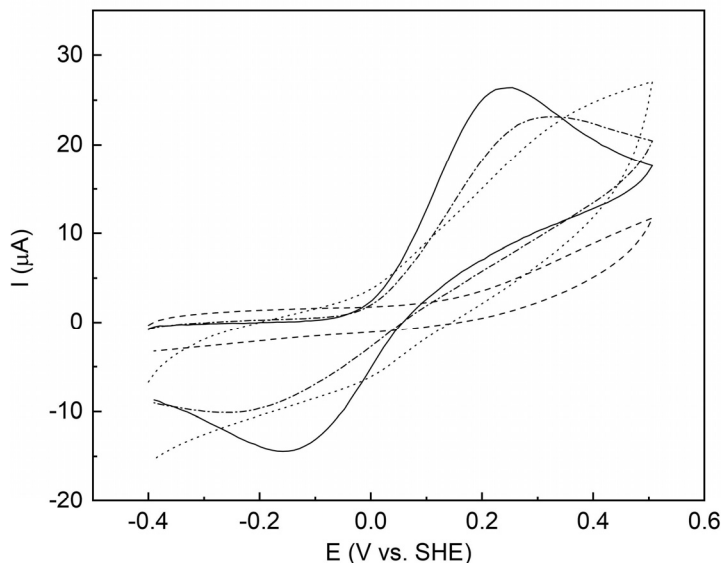


Figure 19. CV for uncoated glassy carbon (solid line), and glassy carbon electrode coated with graphite/polystyrene mixture containing 30% (dashed line), 50% (dotted line) and 55% (dot dashed line) of graphite. Conditions: 100 mV s^{-1} scan rate in $1 \text{ mM } [\text{Fe}(\text{CN})_6]^{4-}$ solution with 1 M KCl as the supporting electrolyte. (Publication 2)

The voltammogram for W_g 30% electrode shows that the surface of the Metal/PS-G composite is passivated, i.e. graphite particles are not in direct contact with the electrolyte solution. At 55% graphite concentration, a clear oxidation peak was observed at 0.3 V (vs. SCE), however the charge transfer kinetics are very slow as was seen from the high peak-to-peak separation value ΔE_p (Figure 19), suggesting that there is electrical insulation around the graphite flakes even at higher graphite flake values. More exposed graphite flakes are undoubtedly present on the electrolyte interface when the graphite concentration is more than 53%, and the initial mechanism of charge transport during cathodic pulse polarization is normal electrochemical reduction, which takes place directly on the cathode surface. It is likely that the insulating film coverage is not optimal at higher graphite concentrations, as was observed from the emission intensity, which started to decline for graphite concentration beyond 30% (Figure 18). However, if this is the case, the amount of exposed graphite particles has to be small, as the CV measurements lacked the oxidation peak for electrodes containing 50% of graphite. Based on all these measurements, it seems that the electron injection to electrolyte solution from PS-G electrodes is based on electron tunnel emission through the insulating layer rather than some kind of field emission from bare carbon particles. Cellulose based composite electrodes can be assumed to have similar properties based on these results and the results obtained with other insulating materials, polyvinyl butyral-CB [71] and PS-CB electrodes. [72]

The electron transport zones in studied composite electrodes are (i) from the metal to conductive carbon particles inside of the insulating film, (ii) between the carbon particles inside the insulating film, and (iii) electron injection/transfer to the aqueous solution. At the metal/composite layer interface, electrons are transferred probably partly by direct contact between metal and carbon particles and partly by tunneling. Inside of the composite layer, the main electron transport mechanism is probably resonance tunnelling. At the composite/electrolyte interface, electrons are likely to be partly transferred directly to the solution species by the exposed carbon particles at the surface, and partly by field assisted direct tunnelling [20,108] when the uppermost particles have a thin insulating film coverage by the insulating material in question. When the carbon particles at the surface have been covered by a thin hydrogen film, direct electron transfer to the solution species stops and only tunneling through the thin insulating film (polymer or hydrogen film/bubble barrier) remains to be the operative electron transfer mechanism to the solution. When the energy of the electrons exceeds the conduction band edge value of water, hydrated electrons will be produced similarly as in the cases of oxide-covered aluminium and silicon electrodes [20,27].

7.2.3 The effect of free radical scavengers and co-reactants on HECL

When hot or hydrated electrons are the primary reducing species in the reactions, and hydroxyl radicals generated from the dissolved oxygen are the primary efficiently oxidizing species, the free-radical scavengers (NO_3^- and NO_2^-) are expected to have a significant effect on the observed emission intensity, when co-reactants are not used. The effect of hydrated electron scavengers NO_3^- and NO_2^- , and co-reactant $\text{K}_2\text{S}_2\text{O}_8$ were studied with Tb(III)-L2/PS-G electrodes (Publication 2), and the effect of $\text{K}_2\text{S}_2\text{O}_8$ and NaN_3 were studied with Tb(III)-L3 with CAP-CB electrodes (Publication 3). (Figure 20)

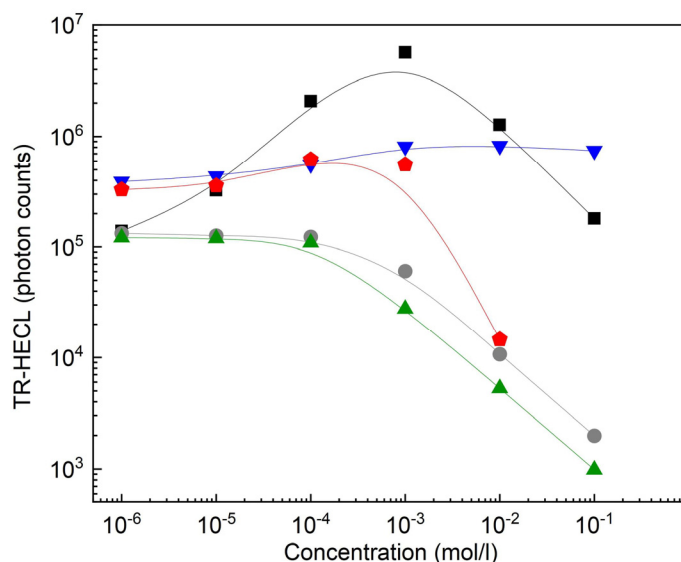


Figure 20. Measured with PS-G electrodes: Effect of electron scavengers: NO_3^- \blacktriangle , NO_2^- \bullet and co-reactant $\text{K}_2\text{S}_2\text{O}_8$ \blacksquare on the TR-HECL intensity in 10^{-5} M Tb(III)-L2. W_g 30 %, 2000 excitation pulses, voltage -35 V, pulse charge 12.6 mC, frequency 20 Hz, delay 0 and gate 4 ms. Interference filter (545 ± 20 nm). (Publication 2) Measured with CAP-CB electrodes: Effect of $\text{K}_2\text{S}_2\text{O}_8$ \blacklozenge and NaN_3 \blacktriangledown on the TR-HECL intensity of 10^{-6} M Tb(III)-L3. W_{cb} 30 %, 2000 excitation pulses, voltage -35 V, pulse charge 9.0 μC , frequency 50 Hz, delay 50 μs and gate 1 ms. Interference filter (550 ± 20 nm). (Publication 3)

TR-HECL decreased two orders of magnitude as a function of NO_3^- and NO_2^- concentration, which shows that PS-G electrodes are usable for generating hydrated electrons and emphasizes the importance of hydrated electrons in the excitation reactions.

From the lowest co-reactant concentrations, it can be seen that the emission without (or with insignificantly low concentration) co-reactants is higher with Tb(III)-L3/CAP-CB than with Tb(III)-L2/PS-G electrodes, and the enhancing effect of the co-reactant is not as strong for Tb(III)-L3. However, with both cases the best $\text{K}_2\text{S}_2\text{O}_8$ concentration was around 10^{-3} M. Azide seems to be a more suitable co-reactant for Tb(III)-L3 than peroxodisulphate. The enhancing effect of azide ion is based on its scavenging action of hydroxyl radicals generated from

dissolved oxygen [20,109], since azidyl radical is a more selective one-electron oxidant for this chelate than hydroxyl radical [20].

The dependency of the TR-HECL signal on the concentration of $K_2S_2O_8$ (Figure 20 squares) is similar to previously published results with different electrode materials such as Al/Al_2O_3 and Si/Si_2O_3 . [67] The addition of persulphate decreases the amount of reducing mediator e_{aq}^- in the system by producing strongly oxidizing sulphate radicals, and when the concentration of peroxydisulphate is increased beyond 10^{-3} M, the HECL emission intensity starts to decrease due to imbalance between oxidizing and reducing equivalents (i.e. $c(e_{aq}^-) \ll (c(SO_4^{\cdot-}))$)[72]. Similar strong decrease in the HECL intensity was not observed at high azide concentrations since it only converts oxidizing species (hydroxyl radicals) to better performing milder oxidizing radicals (azidyl radicals) for $Tb(III)$ -L3.

The ability of composite electrodes to excite different types of HECL excitable luminophores was studied with CAP-CB electrodes. (Publication 2) $K_2S_2O_8$ was used as co-reactant for $Ru(bpy)_3^{2+}$ [26] and NaN_3 for fluorescein [110,111]. The shapes and emission maxima of the spectra are similar as in the literature [107,109,111] which proves that $Ru(bpy)_3^{2+}$, fluorescein and most probably many other HECL labels can be excited at these composite electrodes.

7.2.4 Screen-printed electrodes

Based on the above results and the other studies of these composite materials [67,71,72], EC-CB and PS-CB were chosen to be used in screen-printed electrodes. As the electrodes were being fabricated with this method for the first time, the surface characteristics of the cathode areas in the chips were first analysed by SEM (Figure 21) and AFM, and whole electrode area with surface profiling. (Publication 4)

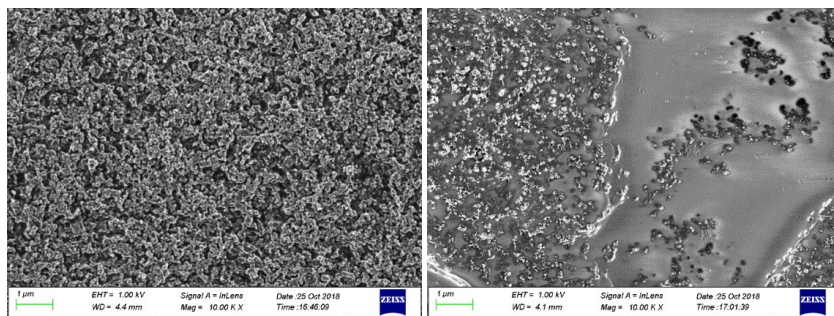


Figure 21. EC-CB (left) and PS-CB (right) electrode surfaces analysed by SEM. Magnification of 10000 times. (Publication 4)

According to SEM studies, the PS-CB electrodes have some areas where the insulating PS and conductive CB are unevenly distributed (Figure 21). The cathode surface of EC-CB electrodes was considerably more uniform than that of PS-CB electrodes. It may be possible that benzyl alcohol, which was chosen as a solvent mainly due to its suitable volatility properties for screen-printing, was not optimal for producing a homogenous PS-CB mixture.

EC-CB and PS-CB electrodes were characterized also by AFM. The mean roughness of EC-CB (54.6 nm, RMS 67.0 nm) and of PS-CB (58.0 nm, RMS 74.2 nm) did not have significant differences, so the actual surface areas of these materials can be assumed to be quite similar and appropriate to be used in immunoassays.

Based on both 2D and 3D profiling, the average height of the CB layer on EC and PS electrodes were very similar, ca. 7–8 μm . The bottom layers of Ag had a thickness of 5–6 μm , which should be able to produce the sufficient conductivity to the bottom layer.

The capability of these electrodes to produce HECL was first tested with 10^{-3} M Tb(III)-L3, and the photographs of emission were taken to observe the spatial location of HECL emission on the working electrodes (Figure 22). In the beginning of the measurement, only the luminophores located near the working electrode edge closer to anode were excited. When pulse polarization (-45 V and 31.5 μC) was continued, whole cathode area was eventually producing HECL. When voltage and charge were too low (e.g. -35 V and 9 μC), emission was seen only in the outer parts and it did not spread in the middle of the electrode during the measurement.

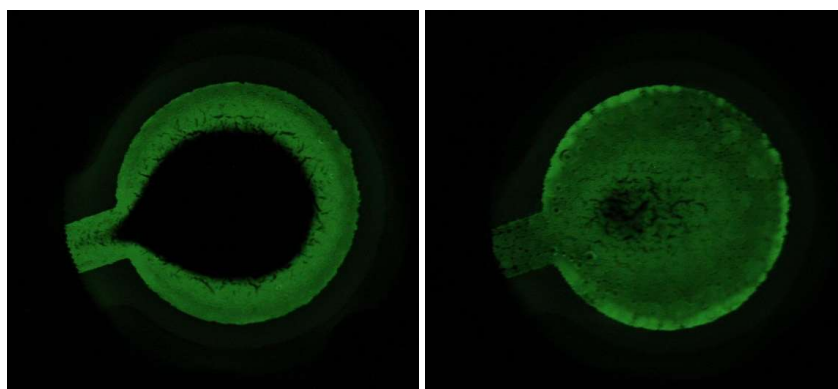


Figure 22. Long exposure photographs, exposure time 1 s. Voltage - 46 V, pulse charge 31.5 μC , frequency 50 Hz. 3 seconds (left) and 29 second (right) after the beginning of the excitation. With 0.01 NaN_3 in 0.05 M $\text{Na}_2\text{B}_4\text{O}_7$, 0.1 M Na_2SO_4 . RS EC-CB electrode. The radius of the working electrode area was the same (3.4 mm) as in Figure 7. (Publication 4)

Based on these observations, the pulse parameters were optimized and the highest emission intensities were observed with RS EC-CB electrodes by applying -

55 V and 31.5 μC . With LF electrode geometry, similar problems were not observed, and the whole area was in use already with lower voltage and charge. However, the emission intensities were lower than with RS electrodes.

The emission intensities of Tb(III)-L3 (left) and FITC (right) as a function of ordinal number of excitation pulses are presented in Figure 23.

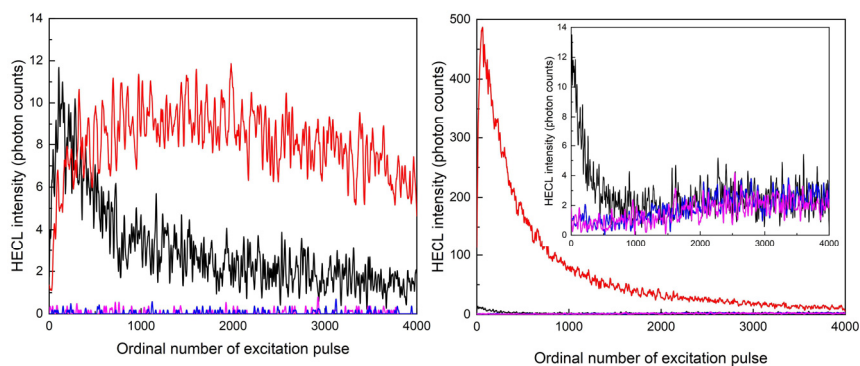


Figure 23. Tb(III)-L3 (left) and FITC (right) with 0.01 NaN_3 in 0.05 M $\text{Na}_2\text{B}_4\text{O}_7$, 0.1 M Na_2SO_4 . RS EC-CB (red), RS PS-CB (black) with 10^{-6} M luminophore. RS EC-CB (blue) and RS PS-CB (purple) without luminophore. Conditions: Pulse charge 31.5 μC , voltage - 55 V, frequency 50 Hz. Interference filter (550 ± 20 nm). Delay 160 μs and gate $4 \cdot 10^{-3}$ s (left). Delay 0 μs and gate $4 \cdot 10^{-5}$ s (right). (Publication 4)

Emission of Tb(III)-L3 was higher with PS-CB electrodes than with EC-CB electrodes in the beginning of the measurement. However, it started to decline after 250 pulses while EC-PS electrodes emission increased until 1000 pulses were measured, and stayed relatively stable for at least 3000 more pulses (Figure 23, left).

With FITC (Figure 23, right), intensities decreased with both electrode materials from the beginning of the measurement, however, the rate of diminishing was slower in the case of EC-CB electrodes, and the intensity was all the time almost 100 times higher than with PS-CB. For some reason, the excitation of FITC is not as effective with PS-CB as it is with EC-CB electrodes. Similar problem was not observed with Tb(III)-L3.

When Tb(III)-L3 and FITC measured with EC-CB are compared, FITC had significantly higher emission intensity than Tb(III)-L, without major background emission. With aluminium electrodes, the analytical applicability of fluorescein is problematic due to high background emission. The measurement of calcein, which belongs to xanthene dye group similarly as fluorescein, showed that the aluminium electrodes exhibited a relatively high electroluminescence background signal during the excitation pulse. This was observed as a poor fit of the calibration curve, and a rather poor detection limit that lies at about $10^{-8} - 10^{-7}$

M, while with PEI-CB composite electrodes it was $3 \cdot 10^{-10}$ M. [67] When lumino- phores with a long luminescence lifetime, such as Tb(III) chelates are measured in time-resolved mode, the background luminescence is avoided and the differ- ence between composite electrodes and aluminium is not as clear. However, the possibility to print the polymer composite electrodes gives easier and wider pos- sibilities for the architecture of such electrodes, compared to aluminium or sili- con as electrode material.

7.2.5 Analytical applicability of composite electrodes

To be able to compare the analytical applicability of the studied electrode mate- rial and fabrication methods, the blank-corrected calibration curves for Tb(III)- L measured with spin-coated PS-G and CAP-CB electrodes and screen-printed EC-CB and PS-CB electrodes are presented in Figure 24.

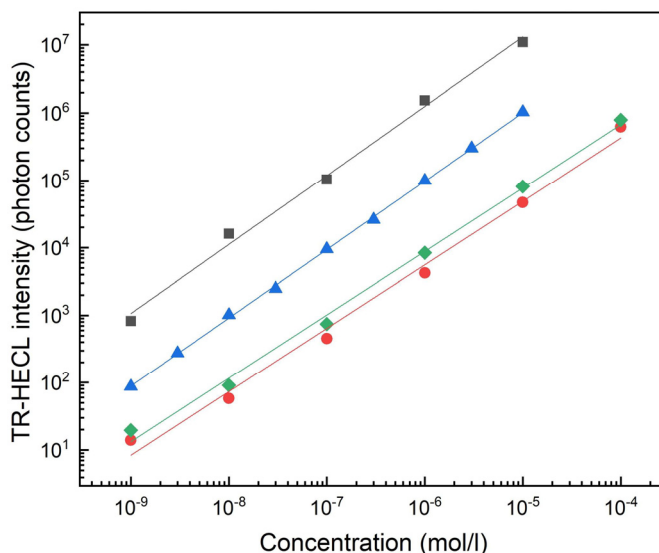


Figure 24. Measured with PS-G electrode ■: Blank corrected calibration curve of Tb(III)-L2. 10^{-3} M $S_2O_8^{2-}$, -35 V, charge 12.6 mC, frequency 20 Hz, Interference filter 545 ± 20 nm (Publication 2). Measured with CAP-CB electrode ▲: Tb(III)-L3 with 0.01 NaN_3 , pulse charge 9.0 μC , voltage -35 V, frequency 50 Hz, delay 50 μs and gate 1 ms. Interference filter 550 ± 20 nm. (Publication 3) Measured with RS EC-CB ◆ and RS PS-CB electrode ●: Calibration curve Tb(III)-L3 with 0.01 NaN_3 . Pulse charge 31.5 μC , voltage -55 V, frequency 50 Hz, delay 160 μs and gate 4 ms. Interference filter 550 ± 20 nm. (Publication 4) Conditions: 0.05 M $Na_2B_4O_7$, 0.1 M Na_2SO_4 , 2000 excitation pulses, $W_{g/cb}$ 30 % except PS-CB which was 40%.

The observed intensities are highest with PS-G and lowest with screen-printed electrodes. However, due to different Tb(III) chelates and measurement param- eters, the comparison of intensities is not as relevant as comparing the detection limits. Blank-corrected calibration curves for FITC measured with EC-CB and PS-CB electrodes are presented in Figure 25. The detection limits and standard deviations of the curves in Figure 24 and Figure 25, and all the other calibration curves in Publications 2-4, are presented in Table 6.

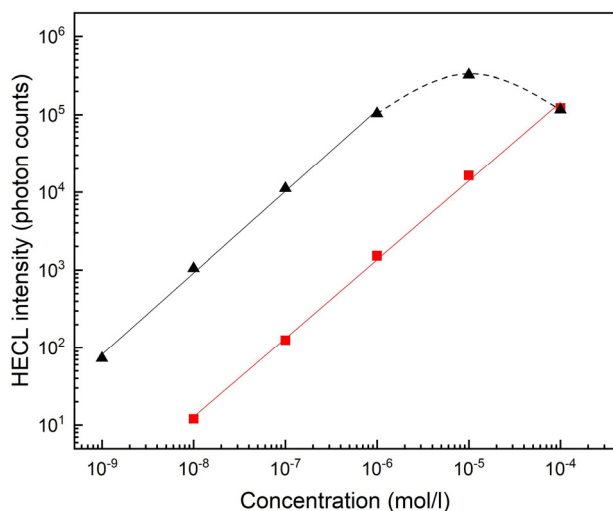


Figure 25. Calibration curve FITC with 0.01 M NaN₃ in 0.05 M Na₂B₄O₇, 0.1 M Na₂SO₄. RS electrode EC-CB ▲ (triangles), PS-CB ■ (squares). Conditions: 500 excitation pulses. In case of EC-CB the light intensity was too high for photon counting above 1 μM solution. Pulse charge 31.5 μC, voltage -55 V, frequency 50 Hz, delay 0 s and gate 40 μs. Interference filter (550±20 nm). (Publication 4)

Table 6. The detection limits and standard deviations of studied luminophores measured with different electrode materials and excitation parameters.

Luminophore/ Electrode material / co-reactant	Excitation	Detection limit	Standard deviation	Publication
Tb(III)-L2 / PS-G / 10 ⁻³ M K ₂ S ₂ O ₈	-35 V, 12.6 μC, 20 Hz	ca. 10 ⁻⁹ M	4 % (10 ⁻⁵ M)	2
Tb(III)-L2 / PS-G / 10 ⁻³ M K ₂ S ₂ O ₈ / DC	DC, 20 V, 60 mA	ca. 10 ⁻⁶ M	23 % (10 ⁻⁵ M)	2
Tb(III)-L3 / CAP-CB / 10 ⁻² M NaN ₃	-35 V, 9.0 μC, 50 Hz	2·10 ⁻¹⁰ M	4 % (10 ⁻⁵ M)	3
Tb(III)-L3 / RS-PS-CB / 10 ⁻² M NaN ₃	-55 V, 31.5 μC, 50 Hz	5·10 ⁻⁹ M	5 % (10 ⁻⁶ M)	4
Tb(III)-L3 / RS-EC-CB / 10 ⁻² M NaN ₃	-55 V, 31.5 μC, 50 Hz	1·10 ⁻⁹ M	2 % (10 ⁻⁶ M)	4
Ru(bpy) ₃ ²⁺ / CAP-CB / 10 ⁻³ M K ₂ S ₂ O ₈	-35 V, 9.0 μC, 50 Hz	4·10 ⁻⁹ M	4 % (10 ⁻⁵ M)	3
FITC / RS-PC-CB / 10 ⁻² M NaN ₃	-55 V, 31.5 μC, 50 Hz	8·10 ⁻⁸ M	12 % (10 ⁻⁶ M)	4
FITC / RS-EC-CB / 10 ⁻² M NaN ₃	-55 V, 31.5 μC, 50 Hz	4·10 ⁻¹⁰ M	10 % (10 ⁻⁶ M)	4
FITC / LF-PS-CB / 10 ⁻² M NaN ₃	-23 V, 67.2 μC, 50 Hz	8·10 ⁻⁸ M		4
FITC / LF-EC-CB / 10 ⁻² M NaN ₃	-23 V, 67.2 μC, 50 Hz	4·10 ⁻⁹ M		4
FITC / RS-EC-CB / 10 ⁻² M NaN ₃	DC, 20 V, 2.5 sec	ca. 10 ⁻⁶ M		4

The lowest detection limit was measured with spin-coated CAP-CB electrodes with Tb(III)-L₃, and almost as good results were obtained with screen-printed EC-CB electrodes with FITC. The results are not fully comparable due to different measurement conditions. The results obtained with screen-printed EC-CB with both RS and LF are promising since the mass ratios of carbon black and polymer were chosen as a compromise between the highest emission intensity and the screen-printing properties of the composite material.

Due to problems with insufficient tolerance of CAP-CB electrodes for incubation in aqueous solution, these electrodes were not used in immunoassays and were

not tested to screen-print. Better adhesion of CAP films to the substrate could have been achieved by using other solvents and optimizing the spin-coating parameters, and with screen-printing there might not have been adhesion problems at all. If the problems with poor adhesion can be solved, the results obtained with CAB-CB electrodes in publication 3 are also encouraging for the further studies, since their emission intensities were higher and electrodes tolerated greater changes in the W_{cb} than CAP-CB or EC-CB electrodes. (Publication 3)

The poor result with screen-printed PS-CB electrodes is possibly related to the uneven distribution of carbon particles and difference in surface properties (hydrophobicity, etc.) of EC and PS. The used W_{cb} might also explain part of the problem. In addition, the pulse parameters were optimized for EC-CB electrodes, which can explain part of the decrease in emission intensity. The results indicate that the manufacturing of these electrodes was not very successful, since with spin-coated PS-CB for Tb(III) chelates detection limit as good as 10^{-10} M has been measured [72]. The applied solvent in making of the composite layer ink should be studied more carefully to obtain more homogenous electrode surface, and the printing method itself was not yet optimal in this first effort of fabrication of printed electrode chips.

The use of direct current excitation was also found to be possible with the present composite electrodes. Thin oxide film-coated electrodes e.g. aluminium cannot be used at all under cathodic DC polarization due to the breakdown of the insulating film [112]. Thus, this is also a promising feature of the present composite materials.

The analytical applicability of cellulose based electrodes was studied next by measuring calibration curves of hCRP with Tb(III)-L4 as a label with spin-coated EC-CB (Publication 3) and screen-printed RS EC-CB (Publication 4) electrodes (Figure 26).

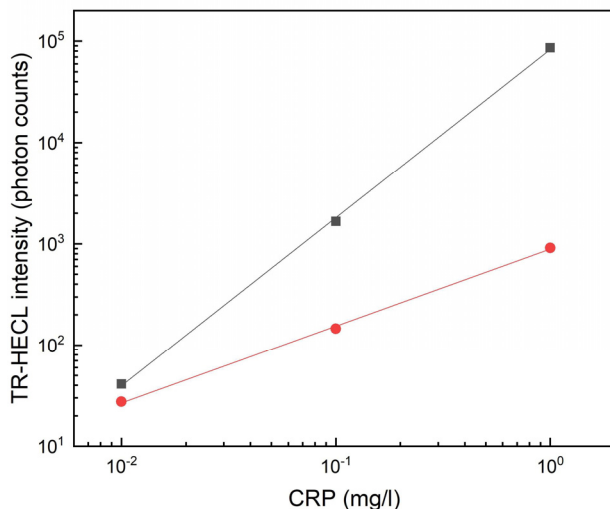


Figure 26. Blank subtracted calibration curves of hCRP with 15 min incubation time and 15 μ l sample volume. 0.01 M NaN_3 in 0.05 M $\text{Na}_2\text{B}_4\text{O}_7$, 0.1 M Na_2SO_4 . 100 ng/cell of antibody labelled with Tb(III)-L4. Conditions: 2000 excitation pulses, frequency 50 Hz, Interference filter 550 ± 20 nm, W_{cb} 30 %. Measured with spin-coated EC-CB electrodes ■, pulse charge 9.0 μC , voltage - 35 V, delay 50 μs and gate 1 ms. (Publication 3) And with screen-printed EC-CB electrodes ●, pulse charge 31.5 μC , voltage - 55 V, delay 160 μs and gate 4 ms. (Publication 4)

The calibration curve of hCRP was measured with FITC as a label at RS EC-CB electrodes (Figure 27). To be able to compare the results, the detection limits and standard deviations of the curves in Figure 26, Figure 27 and all the other immunoassays studied in Publications 3 and 4 are presented in Table 7.

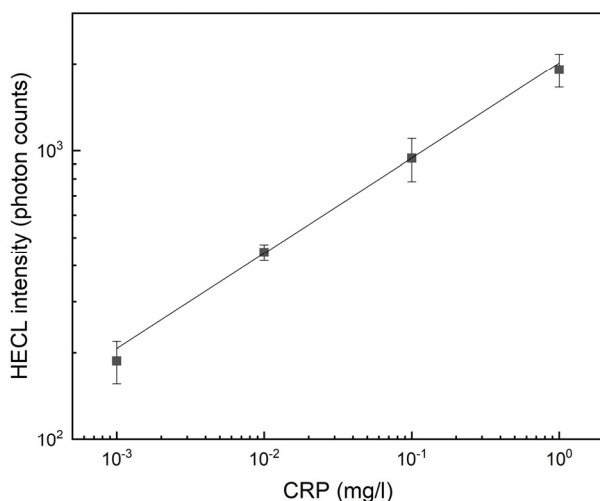


Figure 27. Blank subtracted calibration curves of CRP with 15 min incubation time and 15 μ l sample volume. 0.01 M NaN_3 in 0.05 M $\text{Na}_2\text{B}_4\text{O}_7$, 0.1 M Na_2SO_4 . 100 ng/cell of antibody labelled with FITC. Conditions: 500 excitation pulses, Pulse charge 31.5 μC , voltage - 55 V, frequency 50 Hz, delay 0 μs and gate $4 \cdot 10^{-5}$ s. Interference filter (550 ± 20 nm). Measured with RS EC-CB electrodes. Confidence bars calculated with 95% confidence level, $n=2$. (Publication 4)

Table 7. The detection limits and standard deviations of hCRP measured with different electrode materials and excitation parameters.

Luminophore/ Electrode material / co-reactant	Excitation	Detection limit	Publication
Tb(III)-L4 / EC-CB / 10^{-2} M NaN_3	-35 V, 9.0 μC , 50 Hz	ca. $1 \cdot 10^{-2}$ mg l^{-1}	3
Tb(III)-L4 / RS-EC-CB / 10^{-2} M NaN_3	-55 V, 31.5 μC , 50 Hz	$7 \cdot 10^{-2}$ mg l^{-1}	4
Tb(III)-L4 / RS-PS-CB / 10^{-2} M NaN_3	-55 V, 31.5 μC , 50 Hz	$6 \cdot 10^{-1}$ mg l^{-1}	4
FITC / LF-EC-CB / 10^{-2} M NaN_3	-23 V, 67.2 μC , 50 Hz	$5 \cdot 10^{-2}$ mg l^{-1}	4
FITC / RS-EC-CB / 10^{-2} M NaN_3	-55 V, 31.5 μC , 50 Hz	$6 \cdot 10^{-3}$ mg l^{-1}	4

The calibration curve of hCRP with screen-printed EC-CB electrodes, and with FITC as a label, was linear over three orders of magnitude of concentration and the calculated detection limit ($s/n = 3$) was $6 \cdot 10^{-3}$ mg l^{-1} , which was the best among the studied materials. When Tb(III)-L4 was used as label, spin-coated electrodes gave better results than screen-printed electrodes, which indicates that with spin-coated EC-CB electrode, the detection limit of FITC could have been even lower. With spin-coated PS-CB electrodes, the detection limit was reported to be as low as $3 \cdot 10^{-4}$ mg l^{-1} [72], which makes the poor results of screen-printed PS-CB electrodes even more surprising. In addition, the low HECL intensities and moderate analytical slopes in the hCRP calibration curves measured with screen-printed electrodes needs to be studied further.

Determination of CRP via HECL has been previously studied also with silicon electrodes. With integrated silicon electrodes, the detection limit was ca. $1 \cdot 10^{-3}$ mg L^{-1} [74] and with planar oxide coated silicon electrodes it was as low as $3 \cdot 10^{-4}$ mg l^{-1} [75]. However, the production of these silicon electrodes is expensive and rather difficult due to the need for clean room conditions.

FITC could be detected down to a lower concentration without time-discrimination, than the presently used Tb(III) chelates using time-resolved detection, which is promising for real-world applications. However, extremely sensitive immunoassays do not yet seem obtainable with the present printed electrode chips, since the detection limit of plain label chelates should be of the order of $1 \cdot 10^{-11}$ M to offer sufficient measurement limits for analytes such as the thyroid stimulating hormone. When the best aromatic Tb(III) chelates that are not yet commercially available, are used, the detection limits even with the presently used printed electrode chips can be considerably lowered.

Similar to photoluminescence applications, small sized detectors, even smartphone cameras, can be used as detectors in HECL measurements. In ECLIA only the measurement of luminescence intensity is needed, which simplifies the detection compared to AC measurements with photoluminescence, where the data sets in LTM were much more complicated. In recent years, there has been an exponential increase in the publications on the use of smartphones for e.g. fluorescence and electrochemiluminescence detections in POC diagnostics. [113,114] However, the detected HECL intensities in CRP-immunoassays were quite low, which sets challenges in detection with smartphones. The reason for quite low intensities has been suggested to be that, during cathodic pulse

polarization the catching antibodies are detached from the working electrode surface [61]. This problem could be avoided by using covalent attachment of catching antibodies to the working electrode. Cellulose especially, can be easily modified to bind antibodies due to its functional hydroxyl groups. [115] Also PS can be pretreated in various ways to allow covalent binding of biomolecules to the surface [116].

Inkjet printing by material printers could be considered as a possible method to produce electrodes, as it would allow for printing directly on the appropriate areas of disposable assay's cartridge. Cartridges are much more attractive from the point of view of the users, than the droplet type incubation chips used in this study. However, screen-printed electrode chips can as well be used in assay cartridges. The use of direct current excitation is also a possibility when the instrumentation is required to be simplified even further.

There is still a lot of product development work to be done before a real-world POC application is on the market. The development of the assay cartridge, the optimization of the electrode materials, selecting the best luminophores and the tests with real-blood samples still have to be done, and the whole instrumentation should preferably be miniaturized. However, the possibility to use inexpensive luminophores with short luminescence lifetimes, to mass produce electrodes by printing, to bind catching antibodies covalently to the working electrode, to use inexpensive and more environmentally friendly cellulose materials in electrodes, and also the possibility to use smartphones for the detection in the future, have made the development of low cost POC systems quite a realistic goal.

8. Conclusions

Luminescent markers and labels can be utilized in commercially important applications such as in anti-counterfeiting (AC) and in bioaffinity assays (BA). In AC techniques, the availability of wide variety of luminescent markers together with, the reliability, ease of the use and price of the detection method, are important factors. In addition, the marker must be compatible with the materials used in the product package. Cellulose was found to show long-lived emissions originating from multiple luminescence centres. Process conditions and the chemicals used in the fibrillation, especially TEMPO-oxidation, have an effect on the luminescence centres. However, the actual origin of cellulose luminescence is still far from unambiguous. Multiple chemical characteristics, e.g. hydroxynaphthoquinones, metal ions and possible luminescence quenching and enhancing functional groups, as well as the physical characteristics, such as, crystallinity, should be taken into consideration when the luminescence properties of cellulose are evaluated and cellulose is used in luminescence applications.

Multiple combinations of organic luminophores, lanthanide chelates and inorganic phosphors can be used to create luminescence topography maps (LTM) for verification of the authenticity of the marker. Complex measurement data obtained with laboratory level luminescence spectrometers can be simplified and condensed by just comparing the intensities at the most important emission wavelengths and decay time scales. In addition, the emission properties of cellulose and optical brightening agents can be used in LTM as a natural source of internal standards provided by the packaging material itself. Hand-held AC instruments utilizing both organic and inorganic luminophores as AC markers are becoming realistic in the near future, since the cameras and computing power of the smartphones are constantly evolving. The whole authentication process, from the photoexcitation of the markers to the recognition of the product, was demonstrated with a smartphone application developed in our project. Even more efficient detection can be achieved if an additional microcontroller-based module utilizing powerful UV-LEDs or diode lasers is applied. Authentication by smartphones opens new possibilities for all the consumers to authenticate the products, especially when the technique is combined with other techniques such as QR-codes. The results obtained in our collaboration project give a good basis for the development work towards real-world AC applications.

The goal of the BA development work was to find low-cost alternatives for oxide-coated silicon electrodes and Tb(III) chelate labels. Composite electrodes have good signal to noise ratio and better chemical and physical stability compared to oxide coated inorganic electrodes. Cellulose based composite material is especially well-suited for the fabrication of screen-printed electrodes. The possibility of covalent attachment of catching antibodies to the working electrode surface due to the multiple hydroxyl groups in cellulose is a promising feature. This could also solve the problem of rather low emission intensity obtained with the immunoassay of C-reactive protein. FITC could be detected to a lower concentration without time-discrimination, than the presently used Tb(III) chelates using time-resolved detection, which is very promising for low-cost POC applications due to the very low price of FITC.

The development of low cost POC system seems to be now quite a realistic goal. The possibilities i) to use inexpensive luminophores, ii) to mass produce electrodes by printing, iii) to bind catching antibodies covalently to the working electrode in the future applications, iv) to use inexpensive and more environmentally friendly cellulose materials in electrodes, and v) to use smartphones for the detection and data transfer, all make the development of a low-cost POC system feasible.

References

- [1] J.R. Lakowicz, Principles of Fluorescence Spectroscopy, 3rd ed., Springer, New York, 2006. doi:10.1007/978-0-387-46312-4.
- [2] B. Duong, H. Liu, C. Li, W. Deng, L. Ma, M. Su, Printed Multilayer Microtaggants with Phase Change Nanoparticles for Enhanced Labeling Security, ACS Appl. Mater. Interfaces. 6 (2014) 8909–8912. doi:10.1021/am501668x.
- [3] O. Guillou, C. Daiguebonne, G. Calvez, K. Bernot, A Long Journey in Lanthanide Chemistry: From Fundamental Crystallography Studies to Commercial Anticounterfeiting Taggants, Acc. Chem. Res. 49 (2016) 844–856. doi:10.1021/acs.accounts.6b00058.
- [4] Leonis L. da Luz, R. Milani, J.F. Felix, I.R.B. Ribeiro, M. Talhavini, B.A.D. Neto, J. Chojnacki, M.O. Rodrigues, S.A. Júnior, Inkjet Printing of Lanthanide–Organic Frameworks for Anti-Counterfeiting Applications, ACS Appl. Mater. Interfaces. 7 (2015) 27115–27123. doi:10.1021/acsami.5b06301.
- [5] J.F.C.B. Ramalho, L.C.F. António, S.F.H. Correia, L.S. Fu, A.S. Pinho, C.D.S. Brites, L.D. Carlos, P.S. André, R.A.S. Ferreira, Luminescent QR codes for smart labelling and sensing, Opt. Laser Technol. 101 (2018) 304–311. doi:10.1016/j.optlastec.2017.11.023.
- [6] E. Moretti, G. Pizzol, M. Fantin, F. Enrichi, P. Scopece, M. Ocaña, S. Polizzi, Luminescent Eu-doped GdVO₄ nanocrystals as optical markers for anti-counterfeiting purposes, Chem. Pap. 71 (2017) 149–159. doi:10.1007/s11696-016-0081-8.
- [7] Y. Lu, J. Zhao, R. Zhang, Y. Liu, D. Liu, E.M. Goldys, X. Yang, P. Xi, A. Sunna, J. Lu, Y. Shi, R.C. Leif, Y. Huo, J. Shen, J. a. Piper, J.P. Robinson, D. Jin, Tunable lifetime multiplexing using luminescent nanocrystals, Nat. Photonics. 8 (2014) 32–36. doi:10.1038/nphoton.2013.322.
- [8] Y. Liu, F. Han, F. Li, Y. Zhao, M. Chen, Z. Xu, X. Zheng, H. Hu, J. Yao, T. Guo, W. Lin, Y. Zheng, B. You, P. Liu, Y. Li, L. Qian, Inkjet-printed unclonable quantum dot fluorescent anti-counterfeiting labels with artificial intelligence authentication, Nat. Commun. 10 (2019) 1–9. doi:10.1038/s41467-019-10406-7.
- [9] S. Kalytchuk, Y. Wang, K. Poláková, R. Zbořil, Carbon Dot Fluorescence-Lifetime-Encoded Anti-Counterfeiting, ACS Appl. Mater. Interfaces. 10 (2018) 29902–29908. doi:10.1021/acsami.8b11663.
- [10] K. Jiang, L. Zhang, J. Lu, C. Xu, C. Cai, H. Lin, Triple-Mode Emission of Carbon Dots: Applications for Advanced Anti-Counterfeiting, Angew. Chemie Int. Ed. 55 (2016) 7231–7235. doi:10.1002/anie.201602445.
- [11] M. Li, X. Li, H. Xiao, T.D. James, Fluorescence Sensing with Cellulose-Based Materials, ChemistryOpen. 6 (2017) 685–696. doi:10.1002/open.201700133.
- [12] L. Du, G. He, Y. Gong, W. Zhang, S. Wang, C. Yu, Y. Liua, C. Wei, Efficient persistent room temperature phosphorescence achieved through Zn²⁺ doped sodium carboxymethyl cellulose composites, Compos. Commun. 8 (2018) 106–110. doi:10.1016/j.coco.2017.12.005.
- [13] K. Baatout, F. Saad, A. Baffoun, B. Mahltig, D. Kreher, N. Jaballah, M. Majdoub, Luminescent cotton fibers coated with fluorescein dye for anti-counterfeiting applications, Mater. Chem. Phys. 234 (2019) 304–310. doi:10.1016/j.matchemphys.2019.06.007.
- [14] Q. Wang, J. Cai, K. Chen, X. Liu, L. Zhang, Construction of Fluorescent Cellulose Biobased Plastics and their Potential Application in Anti-Counterfeiting Banknotes, Macromol. Mater. Eng. 301 (2016) 377–382. doi:10.1002/mame.201500364.
- [15] L. Chen, C. Lai, R. Marchewka, R.M. Berry, K.C. Tam, Use of CdS quantum dot-functionalized cellulose nanocrystal films for anti-counterfeiting applications,

- Nanoscale. 8 (2016) 13288–13296. doi:10.1039/c6nr03039d.
- [16] X. Li, Y. Hu, Luminescent films functionalized with cellulose nanofibrils/CdTe quantum dots for anti-counterfeiting applications, *Carbohydr. Polym.* 203 (2019) 167–175. doi:10.1016/j.carbpol.2018.09.028.
- [17] S. Kulmala, C. Mătăchescu, H. Joela, E.-M. Lilius, E.-L. Kupila, UV-irradiated potassium peroxodiphosphate and nitrate as excitation sources for luminol chemiluminescence, *J. Chem. Soc. Faraday Trans.* 93 (1997) 3497–3504. doi:10.1039/a702011b.
- [18] S. Kulmala, T. Ala-Kleme, A. Hakanen, K. Haapakka, F-Centre luminescence from oxide-covered aluminium cathode induced by two-step reduction of peroxydisulfate anions, *J. Chem. Soc. Faraday Trans.* 93 (1997) 165–168. doi:10.1039/a604025j.
- [19] Q. Jiang, H. Ketamo, A.J. Niskanen, J. Suomi, M. Håkansson, S. Kulmala, Effects of thermal oxidation conditions of silicon electrodes on cathodic electrochemiluminescence of Ru(bpy)₃²⁺ chelate, *Electrochim. Acta.* 51 (2006) 3332–3337. doi:10.1016/j.electacta.2005.09.030.
- [20] S. Kulmala, A. Kulmala, T. Ala-Kleme, J. Pihlaja, Primary cathodic steps of electrogenerated chemiluminescence of lanthanide(III) chelates at oxide-covered aluminum electrodes in aqueous solution, *Anal. Chim. Acta.* 367 (1998) 17–31. doi:10.1016/S0003-2670(98)00154-8.
- [21] S. Kulmala, J. Suomi, Current status of modern analytical luminescence methods, *Anal. Chim. Acta.* 500 (2003) 21–69. doi:10.1016/j.aca.2003.09.004.
- [22] B. Valeur, *Molecular Fluorescence: Principles and Applications*, 1st ed., Wiley-VCH Verlag GmbH, 2001. doi:10.1002/3527600248.
- [23] B. Kuswandi, Nuriman, J. Huskens, W. Verboom, Optical sensing systems for microfluidic devices: A review, *Anal. Chim. Acta.* 601 (2007) 141–155. doi:10.1016/j.aca.2007.08.046.
- [24] I. Hemmilä, *Fluoroimmunoassays and Immunofluorometric Assays*, *Clin. Chem.* 31 (1985) 359–370.
- [25] G. V Buxton, C.L. Greenstock, W.P. Helman, A.B. Ross, Critical Review of rate constants for reactions of hydrated electrons, Hydrogen Atoms and Hydroxyl Radicals (OH/O⁻) in Aqueous Solution, *J. Phys. Chem. Ref. Data.* 17 (1988) 513–886. doi:10.1063/1.555805.
- [26] T. Ala-Kleme, S. Kulmala, L. Väre, P. Juhala, M. Helin, Hot Electron-Induced Electrogenerated Chemiluminescence of Ru(bpy)₃²⁺ Chelate at Oxide-Covered Aluminum Electrodes, *Anal. Chem.* 71 (1999) 5538–5543. doi:10.1021/ac981336i.
- [27] J. Suomi, S. Kulmala, Hot Electron-Induced Electrogenerated Chemiluminescence, in: C.D. Geddes (Ed.), *Rev. Fluoresc.* 2009, 1st ed., Springer-Verlag New York, 2011: pp. 47–73. doi:10.1007/978-1-4419-9672-5.
- [28] J. Gooch, B. Daniel, V. Abbate, N. Frascione, Taggant materials in forensic science: A review, *Trends Anal. Chem.* 83 (2016) 49–54. doi:10.1016/j.trac.2016.08.003.
- [29] Y. Duan, M. Liu, W. Sun, M. Wang, S. Liu, Q.X. Li, Recent Progress on Synthesis of Fluorescein Probes, *Mini. Rev. Org. Chem.* 6 (2009) 35–43. doi:10.2174/157019309787316111.
- [30] K. Nishi, S. Isobe, Y. Zhu, R. Kiyama, Fluorescence-Based Bioassays for the Detection and Evaluation of Food Materials, *Sensors.* 15 (2015) 25831–25867. doi:10.3390/s151025831.
- [31] X. Zhang, J. Zhang, L. Liu, Fluorescence Properties of Twenty Fluorescein Derivatives: Lifetime, Quantum Yield, Absorption and Emission Spectra, *J. Fluoresc.* 24 (2014) 819–826. doi:10.1007/s10895-014-1356-5.
- [32] A.-M. Spehar-Déléze, Applications of electrochemiluminescence detection on microfabricated devices, *TKK Dissertations* 44, Helsinki University of Technology, 2006. <http://lib.tkk.fi/Diss/2006/isbn9512283840>.
- [33] M.M. Richter, Electrochemiluminescence (ECL), *Chem. Rev.* 104 (2004) 3003–3036. doi:10.1021/cr020373d.
- [34] I. Hemmilä, V. Laitala, Progress in Lanthanides as Luminescent Probes, *J. Fluoresc.* 15 (2005) 529–542. doi:10.1007/s10895-005-2826-6.
- [35] M.H.V. Werts, Making sense of lanthanide luminescence, *Sci. Prog.* 88 (2005)

- 101–131. doi:10.3184/003685005783238435.
- [36] W.M. Yen, S. Shionoya, H. Yamamoto, eds., *Phosphor handbook*, 2nd ed., CRC Press, Boca Raton, 2006.
- [37] J. Hölsä, Persistent Luminescence Beats the Afterglow: 400 Years of Persistent Luminescence, *Electrochem. Soc. Interface*. 18 (2009) 42–45.
- [38] E.N. Harvey, *A history of luminescence from the earliest times until 1900*, American Philosophical Society, Philadelphia, 1957. doi:10.5962/bhl.title.14249.
- [39] G.F.J. Garlick, A.F. Wells, M.H.F. Wilkins, Zinc Sulfide Phosphor Constitution and Its Effect on Electron Traps, *J. Chem. Phys.* 17 (1949) 399–404. doi:10.1063/1.1747266.
- [40] M. You, M. Lin, S. Wang, X. Wang, G. Zhang, Y. Hong, Y. Dong, G. Jin, F. Xu, Three-dimensional quick response code based on inkjet printing of upconversion fluorescent nanoparticles for drug anti-counterfeiting, *Nanoscale*. 8 (2016) 10096–10104. doi:10.1039/c6nr01353h.
- [41] J. Plimmer, Augmenting and securing the consumer brand experience through smart and intelligent packaging for food, beverages and other fast-moving consumer goods, in: N. Farmer (Ed.), *Trends Packag. Food, Beverages Other Fast-Moving Consum. Goods Mark. Mater. Technol.*, Woodhead Publishing, 2013: pp. 35–57. doi:10.1533/9780857098979.35.
- [42] G. Power, *Anti-counterfeit Technologies for the Protection of Medicines*, Report, World Health Organization (WHO) & International Medical Products Anti-Counterfeiting Taskforce (IMPACT), Geneva, Switzerland, 2008.
- [43] M.R. Carro-Temboury, R. Arppe, T. Vosch, T.J. Sørensen, An optical authentication system based on imaging of excitation-selected lanthanide luminescence, *Sci. Adv.* 4 (2018) 1–7. doi:10.1126/sciadv.1701384.
- [44] F.H. Isikgor, C.R. Becer, *Polymer Chemistry the production of bio-based chemicals and polymers*, *Polym. Chem.* 6 (2015) 4497–4559. doi:10.1039/c5py00263j.
- [45] D. Klemm, B. Heublein, H.-P. Fink, A. Bohn, *Polymer Science Cellulose: Fascinating Biopolymer and Sustainable Raw Material* *Angewandte, Angew. Chemie*. 44 (2005) 3358–3393. doi:10.1002/anie.200460587.
- [46] G.F. Picheth, M.R. Sierakowski, M.A. Woehl, C.L. Pirich, W.H. Schreiner, R. Pontarolo, R.A. de Freitas, Characterisation of ultra-thin films of oxidised bacterial cellulose for enhanced anchoring and build-up of polyelectrolyte multilayers, *Colloid Polym. Sci.* 292 (2014) 97–105. doi:10.1007/s00396-013-3048-0.
- [47] Z. Tang, W. Li, X. Lin, H. Xiao, Q. Miao, L. Huang, L. Chen, TEMPO-Oxidized Cellulose with High Degree of Oxidation, *Polymers (Basel)*. 9 (2017) 1–10. doi:10.3390/polym9090421.
- [48] J. Schmidt, *Electronic Spectroscopy of lignins*, in: C. Heitner, D. Dimmel, J. Schmidt (Eds.), *Lignin Lignans Adv. Chem.*, 1st ed., CRC Press, 2010: p. 683.
- [49] J.A. Olmstead, D.G. Gray, Fluorescence emission from mechanical pulp sheets, *J. Photochem. Photobiol. A Chem.* 73 (1993) 59–65. doi:10.1016/1010-6030(93)80033-6.
- [50] D.L. Mcaleese, R.B. Dunlap, Reduction of Background Emission in Room-Temperature Phosphorescence, *Anal. Chem.* 56 (1984) 600–601. doi:10.1021/ac00267a071.
- [51] T. Bikova, A. Treimanis, UV-absorbance of oxidized xylan and monocarboxyl cellulose in alkaline solutions, *Carbohydr. Polym.* 55 (2004) 315–322. doi:10.1016/j.carbpol.2003.10.005.
- [52] T.P. Nevell, S.H. Zeronian, eds., *Cellulose chemistry and its applications*, Ellis Horwood Ltd; Chichester, 1985.
- [53] R. Atalla, S. Nagel, Laser-induced Fluorescence in Cellulose, *J. Chem. Soc., Chem. Commun.* 19 (1972) 1049–1050. doi:10.1039/C39720001049.
- [54] Y.-Y. Li, B. Wang, M.-G. Ma, B. Wang, Review of Recent Development on Preparation, Properties, and Applications of Cellulose-Based Functional Materials, *Int. J. Polym. Sci.* 2018 (2018) 1–18. doi:10.1155/2018/8973643.
- [55] J. Kim, S. Mun, H. Ko, G. Yun, J. Kim, Disposable chemical sensors and biosensors made on cellulose paper, *Nanotechnology*. 25 (2014) 1–7.

- doi:10.1088/0957-4484/25/9/092001.
- [56] J. Huang, N. Matsunaga, K. Shimanoe, N. Yamazoe, T. Kunitake, Nanotubular SnO₂ Templated by Cellulose Fibers: Synthesis and Gas Sensing, *Chem. Mater.* 17 (2005) 3513–3518. doi:10.1021/cm047819m.
- [57] S. Ummartyotin, H. Manuspiya, A critical review on cellulose: From fundamental to an approach on sensor technology, *Renew. Sustain. Energy Rev.* 41 (2015) 402–412. doi:10.1016/j.rser.2014.08.050.
- [58] G.E. Fridley, C.A. Holstein, S.B. Oza, P. Yager, The evolution of nitrocellulose as a material for bioassays, *MRS Bull.* 38 (2013) 326–330. doi:10.1557/mrs.2013.60.
- [59] V. Fascio, R. Wüthrich, H. Bleuler, Spark assisted chemical engraving in the light of electrochemistry, *Electrochim. Acta.* 49 (2004) 3997–4003. doi:10.1016/j.electacta.2003.12.062.
- [60] E. Santos, W. Schmickler, Electrocatalysis of Hydrogen Oxidation – Theoretical Foundations, *Angew. Chemie Int. Ed.* 46 (2007) 8262–8265. doi:10.1002/anie.200702338.
- [61] K. Salminen, Composite electrodes for hot electron-induced electrochemiluminescence applications, *Doctoral Dissertations 322/2019*, Aalto University, 2019. <http://urn.fi/URN:ISBN:978-952-60-8853-2>.
- [62] S. Kulmala, T. Ala-Kleme, H. Joela, A. Kulmala, Hot electron injection into aqueous electrolyte solution from thin insulating film-coated electrodes, *J. Radioanal. Nucl. Chem.* 232 (1998) 91–95. doi:10.1007/BF02383720.
- [63] A.-H. Wu, J.-J. Sun, X.-L. Su, Y.-W. Lin, Z.-B. Lin, H.-H. Yang, G.-N. Chen, Cathodic electrochemiluminescence at C/CxO(1-x) electrodes for the fabrication of label-free biosensors., *Analyst.* 135 (2010) 2309–2315. doi:10.1039/b924403d.
- [64] T. Ala-Kleme, S. Kulmala, M. Latva, Generation of Free Radicals and Electrochemiluminescence at Pulse-polarized Oxide-covered Silicon Electrodes in Aqueous Solutions, *Acta Chem. Scand.* 51 (1997) 541–546. doi:10.3891/acta.chem.scand.51-0541.
- [65] S. Kulmala, T. Ala-Kleme, L. Heikkilä, L. Väre, Energetic electrochemiluminescence of (9-fluorenyl)methanol induced by injection of hot electrons into aqueous electrolyte solution, *J. Chem. Soc. Faraday Trans. 93* (1997) 3107–3113. doi:10.1039/a702135f.
- [66] M. Håkansson, Q. Jiang, J. Suomi, K. Loikas, M. Nauma, T. Ala-Kleme, J. Kankare, P. Juhala, J.U. Eskola, S. Kulmala, Cathodic electrochemiluminescence at double barrier Al/Al₂O₃/Al/Al₂O₃ tunnel emission electrodes, *Anal. Chim. Acta.* 556 (2006) 450–454. doi:10.1016/j.aca.2005.09.064.
- [67] K. Salminen, P. Grönroos, H. Härmä, S. Kulmala, Hot electron-induced electrochemiluminescence of calcein and calcein-Tb(III) complex at disposable oxide-covered aluminum and polyvinyl butyral-carbon black/metal composite electrodes in aqueous solutions, *Electrochim. Acta.* 266 (2018) 212–219. doi:10.1016/j.electacta.2018.02.016.
- [68] A.J. Niskanen, T. Ylinen-Hinkka, S. Kulmala, S. Franssila, Ultrathin tunnel insulator films on silicon for electrochemiluminescence studies, *Thin Solid Films.* 517 (2009) 5779–5782. doi:10.1016/j.tsf.2009.04.014.
- [69] X. Chen, R. Zheng, S. Qin, J. Sun, Hot electron-induced cathodic electrochemiluminescence at oil film-covered carbon paste electrode and application to nano-molar determination of catechol, *Talanta.* 101 (2012) 362–367. doi:10.1016/j.talanta.2012.09.042.
- [70] A. Hakanen, E. Laine, K. Haapakka, Physical origin of the intrinsic cathodic luminescence of an oxide-covered aluminium electrode, *Europhys. Lett.* 39 (1997) 311–316. doi:10.1209/epl/i1997-00353-8.
- [71] K. Salminen, P. Grönroos, L. Johansson, J. Campbell, S. Kulmala, Hot electron-induced electrochemiluminescence at polyetherimide-carbon black-based electrodes, *Electrochim. Acta.* 237 (2017) 185–191. doi:10.1016/j.electacta.2017.03.212.
- [72] K. Salminen, P. Grönroos, J. Eskola, E. Nieminen, H. Härmä, S. Kulmala, Immunoassay of C-reactive protein by hot electron-induced

- electrochemiluminescence at polystyrene-carbon black composite electrodes, *Electrochim. Acta.* 282 (2018) 147–154. doi:10.1016/j.electacta.2018.06.016.
- [73] A.H. Wu, J.J. Sun, Y.M. Fang, R.J. Zheng, G.N. Chen, Hot Electron Induced Cathodic Electrochemiluminescence at Disposable Screen Printed Carbon Electrodes, *Electroanalysis.* 22 (2010) 2702–2707. doi:10.1002/elan.201000233.
- [74] T. Ylinen-Hinkka, A.J. Niskanen, S. Franssila, S. Kulmala, Immunoassay of C-reactive protein by hot electron induced electrochemiluminescence using integrated electrodes with hydrophobic sample confinement, *Anal. Chim. Acta.* 702 (2011) 45–49. doi:10.1016/j.aca.2011.06.038.
- [75] T. Ala-Kleme, P. Mäkinen, T. Ylinen, L. Väre, S. Kulmala, P. Ihalainen, J. Peltonen, Rapid electrochemiluminoimmunoassay of human C-reactive protein at planar disposable oxide-coated silicon electrodes, *Anal. Chem.* 78 (2006) 82–88. doi:10.1021/ac051157i.
- [76] M. Håkansson, K. Salminen, J. Kuosmanen, J. Eskola, H. Peuravuori, S. Kulmala, Immunoassay of β_2 -microglobulin at oxide-coated heavily doped p-silicon electrodes, *J. Electroanal. Chem.* 769 (2016) 11–15. doi:10.1016/j.jelechem.2016.02.040.
- [77] M. Helin, L. Väre, M. Håkansson, P. Canty, H.P. Hedman, L. Heikkilä, T. Ala-Kleme, J. Kankare, S. Kulmala, Electrochemiluminoimmunoassay of hTSH at disposable oxide-coated n-silicon electrodes, *J. Electroanal. Chem.* 524–525 (2002) 176–183. doi:10.1016/S0022-0728(02)00638-1.
- [78] T. Ala-Kleme, Heterogeneous time-resolved electrochemiluminoimmunoassay of thyroid stimulating hormone with magnetic beads at oxide-covered aluminum electrode, *J. Lumin.* 186 (2017) 183–188. doi:10.1016/j.jlumin.2017.02.035.
- [79] S.K. Vashist, A.G. Venkatesh, E.M. Schneider, C. Beaudoin, P.B. Luppa, J.H.T. Luong, Bioanalytical advances in assays for C-reactive protein, *Biotechnol. Adv.* 34 (2016) 272–290. doi:10.1016/j.biotechadv.2015.12.010.
- [80] A.K. Shrivastava, H.V. Singh, A. Raizada, S.K. Singh, C-reactive protein, inflammation and coronary heart disease, *Egypt. Soc. Cardiol.* 67 (2015) 89–97. doi:10.1016/j.ehj.2014.11.005.
- [81] M. Bessonoff, J. Paltakari, A rapid method for the production of fibrillar cellulose films and an insight on their properties, *Nord. Pulp Pap. Res. J.* 30 (2015) 141–148. doi:10.3183/npprj-2015-30-01-p141-148.
- [82] T. Taniguchi, K. Okamura, New films produced from microfibrillated natural fibres, *Polym. Int.* 47 (1998) 291–294. doi:10.1002/(SICI)1097-0126(199811)47:3<291::AID-PI11>3.0.CO;2-1.
- [83] S. Iwamoto, A.N. Nakagaito, H. Yano, Nano-fibrillation of pulp fibers for the processing of transparent nanocomposites, *Appl. Phys. A Mater. Sci. Process.* 89 (2007) 461–466. doi:10.1007/s00339-007-4175-6.
- [84] M. Pääkko, M. Ankerfors, H. Kosonen, A. Nykänen, S. Ahola, M. Österberg, J. Ruokolainen, J. Laine, P.T. Larsson, O. Ikkala, T. Lindström, Enzymatic hydrolysis combined with mechanical shearing and high-pressure homogenization for nanoscale cellulose fibrils and strong gels, *Biomacromolecules.* 8 (2007) 1934–1941. doi:10.1021/bm061215p.
- [85] S.Y. Lee, S.J. Chun, I.A. Kang, J.Y. Park, Preparation of cellulose nanofibrils by high-pressure homogenizer and cellulose-based composite films, *J. Ind. Eng. Chem.* 15 (2009) 50–55. doi:10.1016/j.jiec.2008.07.008.
- [86] T. Saarinen, M. Lille, J. Seppälä, Technical Aspects on Rheological Characterization of Microfibrillar Cellulose Water Suspensions, in: *Annu. Trans. Nord. Rheol. Soc.*, 2009: pp. 121–128.
- [87] T. Kitaoka, A. Isogai, F. Onabe, Chemical modification of pulp fibers by TEMPO-mediated oxidation, *Nord. Pulp Pap. Res. J.* 14 (1999) 279–284. doi:10.3183/NPPRJ-1999-14-04-p279-284.
- [88] T. Saito, Y. Nishiyama, J.L. Putaux, M. Vignon, A. Isogai, Homogeneous suspensions of individualized microfibrils from TEMPO-catalyzed oxidation of native cellulose, *Biomacromolecules.* 7 (2006) 1687–1691. doi:10.1021/bm060154s.
- [89] S. Fujisawa, Y. Okita, H. Fukuzumi, T. Saito, A. Isogai, Preparation and

- characterization of TEMPO-oxidized cellulose nanofibril films with free carboxyl groups, *Carbohydr. Polym.* 84 (2011) 579–583. doi:10.1016/j.carbpol.2010.12.029.
- [90] J. Schindelin, I. Arganda-Carreras, E. Frise, V. Kaynig, M. Longair, T. Pietzsch, S. Preibisch, C. Rueden, S. Saalfeld, B. Schmid, J. Tinevez, D.J. White, V. Hartenstein, K. Eliceiri, P. Tomancak, A. Cardona, Fiji: an open-source platform for biological-image analysis, *Nat. Methods.* 9 (2012) 676–682. doi:10.1038/nmeth.2019.
- [91] M. Raatikka, LuminoTrace: photoluminescence based product authentication for smartphones, Masters Thesis, Aalto University, 2016. <http://urn.fi/URN:NBN:fi:aalto-201608263028>.
- [92] R.A. Mustalish, Optical brighteners: history and technology, *Stud. Conserv.* 45 (2013) 133–136. doi:10.1179/sic.2000.45.Supplement-1.133.
- [93] A. Castellan, R. Ruggiero, E. Frollini, L. Ramos, C. Chirat, Studies on fluorescence of cellulose, *Holzforschung.* 61 (2007) 504–508. doi:10.1515/HF.2007.090.
- [94] Z. Gavrilov, M., N. Ermolenko, I., A study of cellulose luminescence, *J. Appl. Spectrosc.* 5 (1966) 542–544. doi:10.1007/BF00606982.
- [95] A. Vikkula, J. Valkama, T. Vuorinen, Formation of aromatic and other unsaturated end groups in carboxymethyl cellulose during hot alkaline treatment, *Cellulose.* 13 (2006) 593–600. doi:10.1007/s10570-005-9024-1.
- [96] T. Rosenau, A. Potthast, A. Hofinger, P. Kosma, Isolation and identification of residual chromophores in cellulosic materials, *Macromol. Symp.* 223 (2005) 239–252. doi:10.1002/masy.200550517.
- [97] T. Rosenau, A. Potthast, K. Krainz, Y. Yoneda, T. Dietz, Z.P.I. Shields, A.D. French, Chromophores in cellulose, VI. First isolation and identification of residual chromophores from aged cotton linters, *Cellulose.* 18 (2011) 1623–1633. doi:10.1007/s10570-011-9585-0.
- [98] T. Rosenau, A. Potthast, K. Krainz, H. Hettegger, U. Henniges, Y. Yoneda, C. Rohrer, A.D. French, Chromophores in cellulose, XI: Isolation and identification of residual chromophores from bacterial cellulose, *Cellulose.* 21 (2014) 2271–2283. doi:10.1007/s10570-014-0289-0.
- [99] P. Korntner, T. Hosoya, T. Dietz, K. Eibinger, H. Reiter, M. Spitzbart, T. Röder, A. Borgards, W. Kreiner, A.K. Mahler, H. Winter, Y. Groiss, A.D. French, U. Henniges, A. Potthast, T. Rosenau, Chromophores in lignin-free cellulosic materials belong to three compound classes. Chromophores in cellulose, XII, *Cellulose.* 22 (2015) 1053–1062. doi:10.1007/s10570-015-0566-6.
- [100] B.H. Boo, J.H. Kim, Fluorescence and Fluorescence Excitation Spectroscopy of 5,8-Dihydroxy-1,4-naphthoquinone. Analysis of the Electronic Spectra via the Time-Dependent DFT Calculation, *Bull. Korean Chem. Soc.* 34 (2013) 309–312. doi:http://dx.doi.org/10.5012/bkcs.2013.34.1.309.
- [101] N.S. Zwirchmayr, T. Hosoya, H. Hettegger, M. Bacher, K. Krainz, T. Dietz, U. Henniges, A. Potthast, T. Rosenau, Chromophores from hexeneuronic acids: chemical behavior under peroxide bleaching conditions, *Cellulose.* 24 (2017) 3689–3702. doi:10.1007/s10570-017-1398-3.
- [102] M. Tamatani, Principal phosphor materials and their optical properties, in: W.M. Yen, S. Shionoya, H. Yamamoto (Eds.), *Fundam. Phosphors*, CRC Press, Boca Raton, 2006: p. 352.
- [103] W.Z. Yuan, X.Y. Shen, H. Zhao, J.W.Y. Lam, L. Tang, P. Lu, C. Wang, Y. Liu, Z. Wang, Q. Zheng, J.Z. Sun, Y. Ma, B.Z. Tang, Crystallization-Induced Phosphorescence of Pure Organic Luminogens at Room Temperature, *J. Phys. Chem.* 114 (2010) 6090–6099. doi:10.1021/jp909388y.
- [104] Y. Gong, Y. Tan, J. Mei, Y. Zhang, W. Yuan, Y. Zhang, J. Sun, B.Z. Tang, Room temperature phosphorescence from natural products: Crystallization matters, *Sci. China Chem.* 56 (2013) 1178–1182. doi:10.1007/s11426-013-4923-8.
- [105] L. Du, B. Jiang, X. Chen, Y. Wang, L. Zou, Y. Liu, Y.-Y. Gong, C. Wei, W.-Z. Yuan, Clustering-triggered Emission of Cellulose and Its Derivatives, *Chinese J. Polym. Sci.* 37 (2019) 409–415. doi:10.1007/s10118-019-2215-2.
- [106] Y. Hong, J.W.Y. Lam, B.Z. Tang, Aggregation-induced emission, *Chem. Soc. Rev.* 40 (2011) 5361–5388. doi:10.1039/c1cs15113d.

- [107] Q. Jiang, J. Suomi, M. Håkansson, A.J. Niskanen, M. Kotiranta, S. Kulmala, Cathodic electrogenerated chemiluminescence of Ru(bpy)₃²⁺ chelate at oxide-coated heavily doped silicon electrodes, *Anal. Chim. Acta.* 541 (2005) 157–163. doi:10.1016/j.aca.2004.12.075.
- [108] D.J. Dimaria, E. Cartier, Mechanism for stress-induced leakage currents in thin silicon dioxide films, *J. Appl. Phys.* 78 (1995) 3883–3894. doi:10.1063/1.359905.
- [109] S. Kulmala, T. Ala-Kleme, M. Latva, K. Loikas, H. Takalo, Hot electron-induced electrogenerated chemiluminescence of rare earth(III) chelates at oxide-covered aluminum electrodes, *J. Fluoresc.* 8 (1998) 59–65. doi:10.1007/BF02758238.
- [110] J. Suomi, T. Ylinen, M. Håkansson, M. Helin, Q. Jiang, T. Ala-Kleme, S. Kulmala, Hot electron-induced electrochemiluminescence of fluorescein in aqueous solution, *J. Electroanal. Chem.* 586 (2006) 49–55. doi:10.1016/j.jelechem.2005.09.013.
- [111] T. Ylinen, J. Suomi, M. Helin, T. Ala-Kleme, S. Kulmala, Time-Resolved Detection of Hot Electron-Induced Electrochemiluminescence of Fluorescein in Aqueous Solution, *J. Fluoresc.* 16 (2006) 27–33. doi:10.1007/s10895-005-0023-2.
- [112] M. Håkansson, Q. Jiang, A. Spehar, J. Suomi, M. Kotiranta, S. Kulmala, Direct current-induced electrogenerated chemiluminescence of hydrated and chelated Tb (III) at aluminum cathodes, *Anal. Chim. Acta.* 541 (2005) 171–177. doi:10.1016/j.aca.2004.12.072.
- [113] M. Zarei, Trends in Analytical Chemistry Portable biosensing devices for point-of-care diagnostics: Recent developments and applications, *Trends Anal. Chem.* 91 (2017) 26–41. doi:10.1016/j.trac.2017.04.001.
- [114] M.E. Calabretta M.M., Montali L., Lopreside A., Roda A., (2019) Smartphone-Based Cell Detection, in: G. Thouand (Ed.), *Handb. Cell Biosens.*, Springer, Cham, 2019: pp. 1–16. doi:10.1007/978-3-319-47405-2_98-1.
- [115] Y. Peng, V. Van Gelder, A. Amaladoss, K.H. Patel, Covalent Binding of Antibodies to Cellulose Paper Discs and Their Applications in Naked-eye Colorimetric Immunoassays, *J. Vis. Exp.* 116 (2016) 1–11. doi:10.3791/54111.
- [116] U. Bora, L. Chugh, P. Nahar, Covalent immobilization of proteins onto photoactivated polystyrene microtiter plates for enzyme-linked immunosorbent assay procedures, *J. Immunol. Methods.* 268 (2002) 171–177. doi:10.1016/S0022-1759(02)00212-0.



ISBN 978-952-60-3820-9 (printed)
ISBN 978-952-60-3821-6 (pdf)
ISSN 1799-4934 (printed)
ISSN 1799-4942 (pdf)

Aalto University
School of Chemical Engineering
Department of Chemistry and Materials Science
www.aalto.fi

**BUSINESS +
ECONOMY**

**ART +
DESIGN +
ARCHITECTURE**

**SCIENCE +
TECHNOLOGY**

CROSSOVER

**DOCTORAL
DISSERTATIONS**